Master of Science Thesis

Optimization of Automotive Structure using Variable Stiffness Laminates

SACHIN FRANCIS

Faculty of Aerospace Engineering · Delft University of Technology

TU Delft Delft University of Technology

Optimization of Automotive Structure using Variable Stiffness Laminates

Master of Science Thesis

For obtaining the degree of Master of Science in Aerospace Engineering
at Delft University of Technology

SACHIN FRANCIS

5^{th} July, 2017

Faculty of Aerospace Engineering · Delft University of Technology

The work in this thesis was supported by DES COMPOSITES. Their cooperation is gratefully acknowledged.

Copyright © SACHIN FRANCIS
All rights reserved.

Delft University of Technology
Faculty of Aerospace Engineering
Department of Aerospace Structures and Materials

GRADUATION COMMITTEE

Dated: 5th July, 2017

Chair holder:

Dr.Sergio Turteltaub

Committee members:

Dr.Julien Van Campen

Dr.Daniël Peeters

Dr.Derek Gransden

Abstract

Variable Stiffness Laminates are created by spatially varying the fiber orientation resulting in designs that makes use of curved fibers rather than Uni-directional fibers to tailor the properties to design requirement. The advent of automated manufacturing methods such as Automated Fiber Placement and Tailored Fiber Placement has made variable stiffness laminate more realistic and attractive for use in aerospace and automotive sector. Importance of light weight designs in automotive sector has received new interest due to the stringent emissions rules and entry of designs based on alternative energy. Within this context, this thesis intends to create variable stiffness design for an automotive part to investigate the possible improvements in structural responses compared to a design based on conventional laminates.

The design is done based on 2D Finite element analysis coupled with a convex optimization that helps to generate steered fiber designs optimized for strength, stiffness and buckling. One of the important loadcase studied here is the inertia relief. Inertia Relief analysis is generally applied to unconstrained bodies that undergo rigid body motion (such as a plane in flight or chassis on a suspension) and is of interest for the part studied here. Inertia relief method is implemented in the finite element framework and results are verified for test cases such as beams, rectangular plate and cylinder. The method is then used to analyse the automotive part and the responses from the analysis are taken for optimization.

After completion of finite element analysis for all the loadcases, a gradient based optimization problem is setup for optimizing fiber angle distribution. Together with constraints for structural responses a set of manufacturing constraints are also used during optimization so that realistic fiber angle distributions are achieved at every design points or nodes. To obtain steered fiber paths, the fiber angle distribution after optimization is curve-fitted using a streamline analogy.

Final optimization of the structure showed that significant improvement in the objective responses can be achieved by using variable stiffness laminates over a conventional laminate design(UD). The results also implies that reduction in weight can be achieved if a variable thickness optimization is to be done for the model.

Table of Contents

List of Figures

List of Tables

Nomenclature

List of Symbols

Abbreviations

AFP	Automated Fiber Placement
ATL	Advanced Tape Layup
$CLPT$	Classical laminate plate theory
DES	D'Amato Engineering Solutions
MPC	Multi-point constraint
$RBE2$	Rigid body element
TFP	Tailored Fiber Placement
UD	Uni-directional
VSL	Variable Stiffness Laminates

Greek Symbols

ϵ	Mid-plane strains
κ	Mid-plane strains
ϕ	Sensitivity of reciprocal terms
ψ	SENSITIVITY OF LINEAR TERMS

Latin Symbols

$\mathbf{A}$	In-plane Stiffness
$\mathbf{B}$	Stiffness Coupling Matrix
$\mathbf{D}$	Out-of-plane stiffness
$\mathbf{K}_b$	Global bending stiffness
$\mathbf{K}_g$	Global geometric stiffness
$\mathbf{M}$	Out-of-plane moments
$\mathbf{N}$	In-plane forces
$\mathbf{U}$	Laminate invariants

$\mathbf{V}$	In-plane lamination parameter
$\mathbf{W}$	Out-of-plane lamination parameter
C	Compliance
P_{cr}	Buckling load
T	Transformation matrix
z	Normalized objectives and constraints vector

Acknowledgments

“ The Only Thing That Is Constant Is Change - Heraclitus ” .

Like what happens to most of the theories and rules in this world that get updated over the course of time, my Masters Studies in Delft was all about updating what I knew about engineering and in a way what I knew about myself. The journey culminates in my masters thesis and this report. I am grateful to everyone who supported me throughout this journey.

Most importantly I have to thank my family for giving me this opportunity and unconditional support during what was an enduring and humbling experience.

Next I would like to thank my supervisors (yes, plural). I had the luxury of working with three supervisors, which I believe is a feat in itself. I began my thesis with Dr.Mostafa Abdalla who was my main supervisor until February 2017. I would like to thank him for providing me this topic regarding variable stiffness laminates which was truly something new and an inspiration for me. I must concede that it was difficult to keep up with your thoughts but it was still a great learning experience. A big thanks goes to my daily supervisor Dr.Daniël Peeters for all the hours of consultation and walk in sessions. I had taken it for granted that you will always have time whenever I approached you with a question, despite your PhD work load. Thanks for answering all my questions and help with optimization code. After Dr.Mostafa left Delft, my main supervisor was Dr.Julien van Campen who agreed to add me to his already busy schedule. I thank him for all the help and support during the finishing stages of my thesis .

Friends were family in Delft, thanks to all of them for the nice time during my masters studies it wouldn’t have been the same without you guys.

Farewell.

Delft, University of Technology
5th July, 2017

SACHIN FRANCIS

Chapter 1

Introduction

1.1 Introduction

The Anisotropic properties of composite materials offer a lot of design freedom, especially its tailorablilty. The possibility to orient fibers in any direction in the matrix system have shown promising improvements in strength and weight savings. This is possible because varying the fiber directions spatially helps to vary the local stiffness in a ply which can be utilized to improve the stress distribution. The improvement in buckling,strength and maximum frequency response compared to conventional unsteered laminates (most cases a Quasi-Isotropic laminate)have been quite evident from the previous studies [3] [4] [5] [6]. These studies have reported improvement in stiffness upto 40% without considering any manufacturing constraints and upto 20% with considering the effect of manufacturing constraints(mainly steering limits). Such laminates with spatially varying fibers are called Variable Stiffness Laminates (VSL) or steered fiber laminates in literature.

Variable Stiffness laminates have been in niche of research and development for the past decade, although they are theoretically proven to be much more efficient than Uni-directional (UD) ply laminates it has not been completely realized due to the complexities in manufacturing these designs. Also the amount of design variables that would be present in the optimization makes it really a difficult and computationally expensive process. It can be said that these complexities constrained the early introduction of this technology into industry, considering the fact that automated fibre placement was already conceived in early 1970's [7].

Developments in field of industrial automation made variable stiffness laminates all the more feasible. The late 1970's marked the development of Advanced Tape Layup (ATL) and later followed the Automated Fiber Placement (AFP) technique [7]. AFP was in way a fusion between ATL and filament winding technique that allowed deposition of tows on almost any arbitrary surface. Tailored Fiber Placement (TFP) was introduced in 1990s, which was developed from the existing knowledge of textile stitching [8]. TFP offers lot more freedom to lay fibers as compared to AFP but has its own short-comings. An analysis of these production methods can therefore lead to identification of right manufacturing method for producing the structures.

Manufacturing challenges aside,at the core of variable stiffness design it is an optimization problem. The optimization of material distribution is highly researched and developed field of

engineering. Over the years a lot of design and optimization methods have been developed for composite materials. Efficient ways to reach optimal and manufacturable designs have been found in recent years [3] [9] [10]. This thesis will focus on using the above method(discussed in the coming section) to enhance the performance of automotive structures. In the coming section an overview of the research aim and questions are given, followed by discussion about methodology adopted to fulfill these research questions.

1.2 Research Aim and Objective

Aim The main aim of the research is to develop variable stiffness laminate design for the given automotive part that can potentially be lighter than conventional laminate designs. The end result of this thesis will contribute towards overall reduction in the vehicle weight. Also feasible method of production has to be identified to make design into reality. A representative structure will be optimized to develop a framework that can later be applied to other parts of the automotive structure. Compared to structures analyzed in the literature the structure in context is doubly curved part, therefore the results from this thesis will also be interesting to see how the fiber steering works on complex shaped structures. In short, the main research question can be stated as:

"***Investigate the possible gains of using variable stiffness laminate design as compared to conventional laminate design in an double curved automotive structure***"

For achieving the aim a set of sub-questions are framed to breakdown the work into smaller parts. Main sub questions are followed by supporting questions that raises enough arguments for .

1.2.1 Research Questions for Literature Review

1. What is the feasible manufacturing method?
   (a) What are features of AFP and TFP manufacturing method?
      i. What is the production speed?
      ii. What is the percentage of occurrence of embedded defects?
      iii. What material types can be used?
      iv. What is the cost of the process?
      v. What are the possibilities of scaling up of production?

1.2.2 Research Questions for Thesis

1. What are the design requirements of the structure ?
   (a) What is the critical load case?
   (b) What are strength & stiffness requirements?
   (c) What are the manufacturing requirements?
2. How can inertia relief be modelled to existing Static analysis method?

(a) How can the inertia relief method be verified?

3. How much improvement can be made in mechanical responses of the structure?

1.3 Methodology

The optimization of variable stiffness composites being the main objective it is decided to start off with the existing optimizer that has been developed in TU Delft. The existing optimizer has been tested for various cased such as flat plates and cylindrical surfaces, therefore is a good starting point for this thesis. The optimizer includes a finite element part and an optimization part. The finite element part calculates the responses and the sensitivities, which is then given as an input into the optimization part. The finite element part will be extended in such a way that it can handle the inertia relief loadcase. After modelling all the required loadcases optimization will be done to assess the improvements in mechanical responses with respect to a conventional UD laminate design. The results of optimization will be visualized in the form of steered fiber paths on the surface of the structure.

1.3.1 Finite Element modelling

The finite element part is formulated based on a higher order triangular element which has been verified by previous researches and will be unchanged for this thesis. Although the trias are inferior to quad elements, it is well suited for meshing complex curved geometries without using large number of elements. The model(from D'Amato Engineering Solutions (DES) Composites) comes with a combination of quads, solids and trias, which will be simplified to only tria elements. This will reduce the need to model multiple elements in the current finite element code.

Also considering the limited time span of the thesis the complexity of the layup and number of layers will be reduced sufficiently to meet the time constraint. Angle optimization happens at each layer on every node, therefore computational time will scale up depending on both theses quantities (especially for sensitivity calculation). Therefore coarser models will be preferred to reduce the computational time. The actual structure will be meshed in Hypermesh Optistruct and the mesh will be transferred to the optimization code for the analysis. The model setup is discussed in detail in the chapter 3.

1.3.2 Implementation of Inertia Relief Analysis

The inertia relief loadcase is widely used in automotive sector for analyzing chassis structures to account for the inertial loads on the structure. Inertia Relief analysis will be developed to derive the inertia loads which will then be used in the existing finite element part to calculate the responses. The inertia relief loadcase will be verified with simpler structures such as beams and plates before going to the actual automotive structure. The responses from the inertia relief case will be checked against the commercial codes such as NASTRAN/PATRAN which can handle the inertia relief method . For the actual structure the results of inertia relief from Hypermesh Optistruct will be used for verification.

1.3.3 Optimization

Once the finite element part is setup, the results will be passed on for optimization. The optimization method is adapted from the existing optimizer. The existing optimizer does take into account the constraints of manufacturing method used making the optimized designs manufacturable and realistic. The optimization results will be compared to the inital design and the improvements will be assessed. Finally a critical appreciation of the results will be done in the Results and Discussions section to investigate the scope of the results.

Chapter 2

State of the Art

2.1 Classical Laminate Plate Theory

Classical laminate plate theory ($CLPT$) is a method to analyse composite materials. Classical laminate plate theory is based on the assumption that the laminates are sufficiently thin to assume a plain stress condition which essentially neglects any out-of-plane stresses and therefore the effects of delamination or interlaminar stresses are not considered. The equilibrium equation for CLPT can be written as follows:

$$\begin{pmatrix} [N] \\ [M] \end{pmatrix} = \begin{pmatrix} [A] & [B] \\ [B] & [D] \end{pmatrix} \cdot \begin{pmatrix} [\epsilon^0] \\ [\kappa] \end{pmatrix} \tag{2.1}$$

Here **N** is in-plane forces, **M** is Out-of-plane moments, **A** represents the In-plane Stiffness, and **D** represents Out-of-plane Stiffness of the laminate. The **B** represents the coupling between in-plane and out-of-plane stiffness. Terms ϵ and κ represents mid-plane strains and mid-plane curvatures respectively. Expanding the above equation with full formed matrices,

$$\begin{pmatrix} N_x \\ N_y \\ N_xy \\ M_x \\ M_y \\ M_xy \end{pmatrix} = \begin{pmatrix} A_{11} & A_{12} & A_{16} & B_{11} & B_{12} & B_{16} \\ A_{21} & A_{22} & A_{26} & B_{21} & B_{22} & B_{26} \\ A_{16} & A_{26} & A_{66} & B_{16} & B_{26} & B_{66} \\ B_{11} & B_{12} & B_{16} & D_{11} & D_{12} & D_{16} \\ B_{21} & B_{22} & B_{26} & D_{21} & D_{22} & D_{26} \\ B_{16} & B_{26} & B_{66} & D_{16} & D_{26} & D_{66} \end{pmatrix} \cdot \begin{pmatrix} {\epsilon_x}^0 \\ {\epsilon_y}^0 \\ {\epsilon_{xy}}^0 \\ \kappa_x \\ \kappa_y \\ \kappa_{xy} \end{pmatrix} \tag{2.2}$$

These terms can be derived from the orthotropic stiffness matrix (Q) of the given material (assuming the ply is orthotropic in nature which is true for standard composite tapes and UD plies).

$$\begin{aligned} \mathbf{A} &= \int_{-h/2}^{-h/2} Q dz \\ \mathbf{B} &= \int_{-h/2}^{-h/2} z \cdot Q dz \\ \mathbf{D} &= \int_{-h/2}^{-h/2} z^2 \cdot Q dz \end{aligned} \tag{2.3}$$

here the stiffness matrix can be derived from material stress-strain equilibrium equation $\sigma = Q \cdot \epsilon$ considering a plane stress condition. The stress strain equation for plane strain condition is given as follows:

$$\begin{pmatrix} \sigma_x \\ \sigma_y \\ \sigma_x y \end{pmatrix} = \begin{pmatrix} Q_{11} & Q_{12} & 0 \\ Q_{21} & Q_{22} & 0 \\ 0 & 0 & Q_{66} \end{pmatrix} \cdot \begin{pmatrix} \epsilon_x \\ \epsilon_y \\ \epsilon_{xy} \end{pmatrix} \tag{2.4}$$

The stiffness matrix Q can be found out from the material properties ($E1, E2$ and μ_{12}). The above equations are basis of composite stress analysis in finite element methods, where the important difference with respect to isotropic material is the use of ABD matrices instead of Q to formulate the stiffness matrix K (K, from $KU = F$). The difference in the . The details of stiffness matrix Q can be found in any composite handbook or textbook such as [11], where each term in Q matrix and the transformation matrices needed to transform the stiffness matrix to material coordinate system are given.

2.2 Lamination Parameters

A more compact notation of the composite laminate layup is proposed by Tsai and Hahn [12]. A layup with any number of layer can be represented using the set of lamination parameters proposed by the authors. This is beneficial since it can reduce the computational cost by reducing the number of design variables. The representation of in-plane lamination parameters $\mathbf{V}$ and out-of plane lamination parameters $\mathbf{W}$ is as follows:

$$\begin{aligned} &(V_1, V_2, V_3, V_4) \\ &= \int_{-1/2}^{-1/2} (\cos 2\bar{\theta(z)}, \sin 2\bar{\theta(z)}, \cos 4\bar{\theta(z)}, \sin 4\bar{\theta(z)}) d\bar{(z)} \end{aligned} \tag{2.5}$$

$$\begin{aligned} &(W_1, W_2, W_3, W_4) \\ &= \int_{-1/2}^{-1/2} \bar{z}^2 (\cos 2\bar{\theta(z)}, \sin 2\bar{\theta(z)}, \cos 4\bar{\theta(z)}, \sin 4\bar{\theta(z)}) d\bar{(z)} \end{aligned} \tag{2.6}$$

here $\bar{z} = \frac{z}{h}$ is the normalized z coordinates of the ply with respect to thickness h. The in-plane and out-of-plane stiffness matrices can be written using lamination parameters as follows,

$$A = \ = h \cdot (\mathbf{\Gamma_0} + \mathbf{\Gamma_1} \cdot V_1 + \mathbf{\Gamma_2} \cdot V_2 + \mathbf{\Gamma_3} \cdot V_3 + \mathbf{\Gamma_4} \cdot V_4 \tag{2.7}$$

$$D = = \frac{h^3}{12} \cdot (\mathbf{\Gamma_0} + \mathbf{\Gamma_1} \cdot W_1 + \mathbf{\Gamma_2} \cdot W_2 + \mathbf{\Gamma_3} \cdot W_3 + \mathbf{\Gamma_4} \cdot W_4 \tag{2.8}$$

here Γ matrices are defined in terms of material invariants (U) as

$$\Gamma_0 = \begin{pmatrix} U_1 & U_4 & 0 \\ U_4 & U_1 & 0 \\ 0 & 0 & U_5 \end{pmatrix} \Gamma_1 = \begin{pmatrix} U_2 & 0 & 0 \\ 0 & -U_2 & 0 \\ 0 & 0 & 0 \end{pmatrix} \tag{2.9}$$

$$\Gamma_2 = \begin{pmatrix} 0 & 0 & \frac{U_2}{2} \\ 0 & 0 & -\frac{U_2}{2} \\ \frac{U_2}{2} & \frac{U_2}{2} & 0 \end{pmatrix} \Gamma_3 = \begin{pmatrix} U_3 & -U_3 & 0 \\ -U_3 & U_3 & 0 \\ 0 & 0 & -U_3 \end{pmatrix} \tag{2.10}$$

$$\Gamma_4 = \begin{pmatrix} 0 & 0 & U_3 \\ 0 & 0 & -U_3 \\ U_3 & -U_3 & 0 \end{pmatrix} \tag{2.11}$$

The laminate invariants **U** can be given as:

$$U_1 = \frac{3 \cdot Q_{11} + 3 \cdot Q_{22} + 2 \cdot Q_{12} + 4 \cdot Q_{66}}{8} \tag{2.12}$$

$$U_2 = \frac{Q_{11} - Q_{12}}{2} \tag{2.13}$$

$$U_3 = \frac{Q_{11} + Q_{22} - 2 \cdot Q_{12} - 4 \cdot Q_{66}}{8} \tag{2.14}$$

$$U_4 = \frac{Q_{11} + Q_{22} - 6 \cdot Q_{12} - 4 \cdot Q_{66}}{8} \tag{2.15}$$

$$U_5 = \frac{Q_{11} + Q_{22} - 2 \cdot Q_{12} + 4 \cdot Q_{66}}{8} \tag{2.16}$$

If variable stiffness laminate optimization is formulate with lamination parameters as its design variable, the optimized fiber angles have to be traced back. A feasible region of the lamination parameters are set inside which the stacking sequence can be retrieved. The feasibility condition can be found from the works of Bloomfield et.al [13]. Interested readers are referred to the authors work for more details. For this thesis the design variables are fiber angles, lamination parameters is only used for formulating stiffness matrices.

2.3 Variable Stiffness laminates

The design and optimization of Variable stiffness laminates stems back from the 1980's [3]. Optimization of laminates from the conventional layup designs has been already shown beneficial by early researches by Setoodeh et.al [14]. Their method of iterative reorientation of fiber angles until it reach an optimum has already shown improvement compared to Uni-directional layup patterns. One of the drawback of the method was however the formulation of optimization in terms of fiber angles resulted in no-convex functions which often resulted in local optimal solutions. Although they have shown that considerable improvement can be achieved even with a local optimum solution as compared to the initial point. A good step of improvement was found later by Setoodeh et.al [3] in later works where an convex formulation of the function was obtained by using lamination parameters(LP) as design variable. This resulted in a more

robust method where the number of design variables where limited regardless of the layup and solutions closer to global optimum were found in later researches. The maximization of buckling load and maximization of strength using the lamination parameters have been done in [4] and [5] respectively which showed the convex nature of the optimization problem as in the feasible domain of lamination parameter space. To convert the design obtained from optimum distribution of LP's to a set of angles or a layup would therefore be required in this method.

This work has been later on extended by other researchers [9] [10] [15] who tried to better the robustness and effectiveness of the solution by taking into account the manufacturability of the layups. The necessity of the manufacturing constraints arise from the fact that fiber angles retrieved from the optimization of LP's often results in infeasible designs without additional constraints. Therefore an additional constraint similar to strength and buckling have been added in the above works to reach a feasible solution. The manufacturing constraint is formulated based on the fiber placement technology used for production. The machine dynamics will restrict the curvature of the plies to a certain limit. This limit is taken into account by giving a average curvature constraint per layer.

The next step is to generate fiber paths from the results of optimization. A linearly varying fiber angle path design was proposed by Gürdal et.al [16] which showed simple way to build curved fibers. A variable stiffness laminate can be designed by setting a reference path using the two angles and then shifting the subsequent fibre paths in y-direction as shown in Figure 2.1.

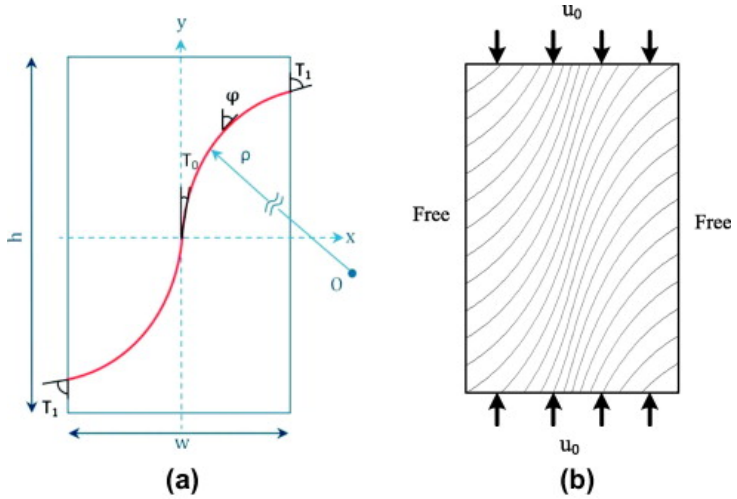

Figure 2.1: Variable stiffness laminate definition (a)reference path (b)shifted fiber paths [17]

One of the problem with above method was the thickness build up in the inflow and outflow (start and stop regions of fiber path). The Fiber path retrieval has been studied in past by various other authors, among them a curve fitting method was proposed by Blom et.al [18] using a streamline analogy that results in fiber paths that looks like streamlines. Here the manufacturing constraints are implemented in the optimization similar to [10] and the resulting distribution of angles are curve fitted to match the streamline function which also smoothen the thickness build up. This method is currently implemented in the TU Delft Optimizer and will be used for thesis, for reading more about stream functions readers are refereed to the work by Blom et.al [18].

In short, the design process can be summarized into three steps :

1. Finding Optimal stiffness distribution

2. Generating the true fiber angle distribution

3. Generating fiber paths from fiber angle distribution

The three step approach shown by the authors above have shown considerable improvement in the mechanical performance of the laminate and is more robust and can be applied to the problem in hand. Although the retrieval of true fiber angles for the given set of lamination parameters will not be done for the thesis, since the improvement with this step has been shown to be minimal [1]. A fiber angle distribution satisfying the feasible domain constraints and manufacturing constraints will be used instead of the true angle.

In the next section a closer look at the manufacturing methods and their features are given and the feasibility of these methods are studied.

2.4 Structural Optimization

Material optimization is a research field active for several decades. Optimization of composite materials has gained importance due to the anisotropic nature of the material. Optimization methods have a common skeleton, it involves a function that is to be optimized (either minimized or maximized depending on the objective), and certain constraints that are to be not violated. The function is formulated in terms of design variables of interest (such as structural dimensions, weight or fiber angle) and the objectives and constraints can be for example structural responses such as strength and buckling or structural dimensions. Depending on the premises of optimization the above setup can vary to suit the problem in hand. A classic example of optimization problem is shown below:

$$\begin{aligned} min \quad & f(x) \\ s.t \quad & h(x) > h_0 \\ & g(x) \leqslant g_0 \end{aligned} \tag{2.17}$$

here $f(x)$ is the optimization function , $h(x)$ is the objective that must be greater than the initial state of h denoted by h_0 .Similarly constraints $g(x)$ must be less than g_0.

2.4.1 Optimization setup for VSL

The VSL optimizer used in this thesis is based on a gradient based optimization method. Gradient based methods are computationally inexpensive than evolutionary algorithms(such as Genetic Algorithm's) and therefore are good choice for problems involving large number of design variables(such as variable stiffness laminate design problems). The gradient based optimization method chooses the direction of descent or direction of search using the gradient of the optimization function. The optimization function is updated iteratively until the improvement in the objectives are negligible. The setup of optimization is formulated based on the min-max type optimization as shown in the Section 2.4.

There are several approaches possible for implementing a gradient based method. In the current optimizer a method of multi-level optimization using structural approximations is used. The optimization function representing structural responses such as strength and buckling is expressed using structural approximations in this method. The multi-level method has shown

to be computationally less expensive in the comparison study performed by van Keulen and de Wit [19]. This method has been used in Phd thesis of Samuel IJsselmuiden [20] performed in TU Delft and has been later on adopted by other researchers showing its validity.

To use the structural approximations to represent optimization functions, it has to comply with certain properties. Four properties that are required to make the optimization more robust are mentioned below:

1. Convexity : an approximation can be called convex, if there is always a unique optimum point for the function. This means for any two points x_1 and x_2 in the feasible domain,

$$f(tx_1 + (1-t)x_2) \leq tf(x_1) + (1-t)f(x_2) \tag{2.18}$$

   where t ranges from 0 to 1

2. Separable : an approximation is separable if it can be expressed as summation of functions of design variables. This is means that the different design variables independent of each other making it efficient. The separable nature of an approximation can be expressed as follows:

$$f(x) = \sum_i f_i(x_i) \tag{2.19}$$

3. Conservative : an approximation is conservative if the value of approximation is less than or equal to the function at the same point. This makes sure that the approximation values stays within the bounds of function value and doesn't exceed the feasible domain. Mathematically it can be represented as follows:

$$f(x) \leq \hat{f}_i(x_i) \tag{2.20}$$

4. Homogeneous : an approximation is homogeneous if its values can be scaled when the design variables values are scaled. This guarantees that feasible point can be reached when the design variables are scaled in appropriate direction.

$$f(\lambda x) = \lambda^n f(x) \tag{2.21}$$

Out of these four, convexity is the only required property for the method of successive approximation used in the current optimizer. The rest of the properties are however highly desirable for efficient approximation.

In the early version of the optimizer a primal-dual problem was solved using the above setup to find new optimum point [20]. In the recent improvements brought by Peeters et.al [10] an interior point method has been implemented owing to increase in number of constraint due to implementation of manufacturing constraint (that are enforced per node). The updated version of the optimizer will be used for this thesis. Interior point method is commonly used in linear programming(LP) problems that helps to identify the minimum by constructing a log barrier function along the constraints. Efficiency of the optimization results depends on how good the barrier functions are. The optimization problem starts with the min-max formulation, the main aim is to minimize the worst response in the given set of responses:

$$\begin{aligned} &min \qquad max(f_1, f_2, ..., f_n) \\ &s.t \qquad f_{n+1}, ...f_m \leqslant 0 \\ &\qquad \varsigma^2 - \varsigma_U^2 \leqslant 0 \end{aligned} \tag{2.22}$$

As seen above, the general setup of an optimization problem involves three main ingredients optimization **function**, **objectives** and **constraints**. The functions f_1 upto f_n represents the structural responses that are to be optimized. And responses f_{n+1} upto f_m represents the constraint responses that are to be maintained throughout the optimization. ς represents the steering value per node and ς_U is the upper bound for the steering set by the manufacturing method (namely AFP and TFP, see Section 2.5 to check steering constraints). It is to be noted here f is the inverse of the responses and therefore the worst response will be $\max(f_1...f_n)$.

Responses

Function that represents the structural responses will be calculated from FEA of the DES model. For the problem in hand three responses are of interest namely: strength,stiffness and buckling . Since the optimization is minimization problem, inverse of the responses needs to be used. Therefore stiffness becomes compliance C and can be calculated as follows:

Compliance

$$C = \frac{1}{Stiffness} = \frac{1}{2}U^T \cdot K \cdot U \tag{2.23}$$

where U represents displacement and K represents the global stiffness matrix.

Buckling Buckling load (P_{cr}) can be calculated using the eigenvalue analysis involving global bending stiffness $\mathbf{K}_b$ and global geometric stiffness$\mathbf{K}_g$.

$$(\mathbf{K}_b - \lambda \mathbf{K}_g) \cdot \mathbf{a} = 0 \tag{2.24}$$

here λ is the buckling factor and $\mathbf{a}$ buckling mode. For the minimization problem the P_{cr} can be written as inverse of the buckling factor.

$$\mathbf{P_{cr}} = \frac{1}{\lambda} \tag{2.25}$$

strength : strength is calculated based on Tsai-Wu failure criteria. The strains in the laminate is used to formulate a failure index (r) which is used instead of stress values. The calculation of failure index has been done by Khani et.al [4], interested readers are refereed to authors work for derivations of the failure index. The linearized form of r used in this thesis is shown below:

$$r \approx \epsilon^T \cdot \mathbf{g}^{(k)} \tag{2.26}$$

where,

$$\mathbf{g}^{(k)} = \frac{\partial r}{\partial \epsilon} \tag{2.27}$$

$$\epsilon = \mathbf{A}^{-1} \cdot \mathbf{N} \tag{2.28}$$

In the multi-level approximation approach two approximations are made namely level one and level two. The level one approximation is in terms of laminate stiffness **A** and **D**. And the level two approximation is derived from level one approximation which is explained below in detail.

Level one approximation

The level one approximation is formulated using convex linearization approach. The convex linearization (ConLin) method proposed by Fleury [21] employs both direct and reciprocal terms to get a convex separable approximation. The stiffness matrices **A** and **D** and their reciprocals are multiplied with their sensitivities (factor that shows importance of its coefficient with respect to other design points) and summed over the domain. Sensitivities shows the change in the responses for a small change in design variable ($\partial f/\partial x$). The formulation of sensitivities is presented in the PhD thesis of Daniël Peeters [1] interested readers are referred to authors work for more details.

$$f^{(1)} = \sum_n \phi_m : \mathbf{A}^{-1} + \phi_b : \mathbf{D}^{-1} + \psi_m : \mathbf{A} + \psi_b : \mathbf{D} + c \tag{2.29}$$

Here the ':' operator represents a Frobenius inner product ($A : B = trace(A^T \cdot B)$). The coefficients of the reciprocal and linear approximation terms ϕ and ψ are computed from the sensitivity analysis [22]. The subscripts m and b represents membrane and bending parts. The optimization runs over all the nodes n. The above approximation is always convex and free term 'c' is the constant part which is zero if there is no inhomogeneous part for the function.

Level two approximation in terms of fiber angles

The level two approximation is derived from the level one approximation as mentioned before in terms of fiber angles. Peeters [1] proposes a similar level two approximation in terms of fiber angle densities which is necessary to implement the topology optimization of variable thickness optimization. In this thesis however focus is only on the fiber angle optimization or variable stiffness optimization. The level two approximation for the optimization is as follows:

$$f^{(2)} = f_0^{(1)} + \mathbf{g} \cdot \Delta\theta + \frac{1}{2} \cdot \Delta\theta^T \cdot \mathbf{H} \cdot \Delta\theta \tag{2.30}$$

Here (g) and (H) is the gradient and Hessian of the level one approximation at the approximation point. For calculation of the derivatives the stiffness matrices are expressed in terms of fiber angle (θ). The level one function is rewritten in terms of fiber angles to compute the level two approximation.

$$f^{(2)}(\theta) = f_0^{(1)}(s(\theta)) \tag{2.31}$$

Here the '$s(\theta)$' represents stiffness matrix in terms of fiber angle. Making use of the above substitution, the gradient of the function can be expressed as follows:

$$g_i = \frac{\partial f^{(1)}}{\partial \theta_i} = \frac{\partial f^{(2)}}{\partial \theta_i} = \frac{\partial f^{(1)}}{\partial s_\alpha} \cdot \frac{\partial s_\alpha}{\partial \theta_i} \tag{2.32}$$

Similarly, Hessian can be found by differentiating twice the level one function,

$$H_i j = \frac{\partial^2 f^{(1)}}{\partial \theta_i \cdot \partial \theta_j} = \frac{\partial^2 f^{(1)}}{\partial s_\alpha \cdot \partial s_\beta} \cdot \frac{\partial s_\alpha}{\partial \theta_i} \cdot \frac{\partial s_\beta}{\partial \theta_j} + \underline{\frac{\partial f^{(1)}}{\partial s_\alpha} \cdot \frac{\partial^2 s_\alpha}{\partial \theta_i \cdot \partial \theta_j}} \tag{2.33}$$

Here the underlined term in equation 2.33 is neglected to make the function convex since it is not positive definite. The remaining gauss-newton part is positive semi-definite and therefore satisfies the convexity property.

Manufacturing Constraints

Manufacturing constraints are imposed during the optimization to guarantee the manufacturability of the layups. This is done by taking into account the variation in fiber angle distribution in adjacent nodes [10]. The gradient of the angle is subjected to a inequality condition, that checks if the fiber angle variation is exceeding the steering limit of the machine. In the work of Peeters et.al [10] a global steering and local steering constraint can be seen. The author mentions the importance of local steering to achieve full guarantee on the manufacturability of the constraint. However using local constraint (one per node instead of one per layer as in global constraint) increases the computational time considerably for the problem in hand. Therefore only a global constraint will be used in this thesis. The formulation of the global constraint is shown below:

$$\varsigma^2 = \nabla\theta \cdot \nabla\theta \tag{2.34}$$

The global steering can be expressed as average steering of the domain.

$$\hat{\varsigma}^2 = \frac{1}{\Omega}\int_{\Omega} \nabla^2 d\Omega \tag{2.35}$$

In a discretized FE domain this can be changed to summation over all the nodes , and can be written as follows:

$$\hat{\varsigma}^2 = \frac{2}{\Omega} \cdot \theta^T \cdot L \cdot \theta \tag{2.36}$$

here L represents the laplacian of the FE domain. In the case of a local constraint L in the above equation will have to be changed to L_e which is laplacian of the element.

Predictor-Corrector Interior point method

The optimization of the level two approximation problem stated in Section 2.4.1 is the main sub-problem that optimizes the fiber angle with the above specified manufacturing constraint. The min-max formulation of the optimization will be rewritten using bound formulation as follows:

$$\begin{aligned} &min \quad && z \\ &s.t \quad && \mathbf{f} - z \cdot \mathbf{e} \leq 0 \\ & && \varsigma^2 - \varsigma_U^2 \leqslant 0 \end{aligned} \tag{2.37}$$

here $\mathbf{e}$ is vector that contains 1's and 0's , where 1's correspond to objectives functions and 0's correspond to constraint functions. In predictor corrector method the inequality constraints that comes from the min-max will be rewritten to equality constraints but with a slack variable $\mathbf{s}$ that ensures that the

$$\begin{aligned} min \quad & z \\ s.t \quad & \mathbf{f} - z \cdot \mathbf{e} + \mathbf{s_0} = 0 \\ & \varsigma^2 - \varsigma_U^2 + \mathbf{s_c} = 0 \end{aligned} \tag{2.38}$$

The lagrangian of the problem can be written as follow:

$$\begin{aligned} \mathcal{L}(\lambda_0, \lambda_c, \theta, z, s_0, s_c) = z + \lambda_0 \cdot (f - z \cdot e^T + s_0) \\ +\theta^T \cdot (\lambda_c \cdot \mathbf{L}) \cdot \theta - {\varsigma_U}^2 \cdot (\lambda_c \cdot |\Omega|) \\ +\lambda_c \cdot s_c |\Omega|) \\ -\mu \cdot (\ln(s_0) + |\Omega| \cdot \ln(s_c)) \end{aligned} \tag{2.39}$$

where λ_0 and λ_c are the lagrange multipliers of the functions(i.e responses) and constraints. And homotopy factor is depicted by μ. To find the optimal point the gradient of the Lagrangian has to be set to zero. The gradient is calculated with respect to $\lambda_0, \lambda_c, \theta, z, s_0, s_c$ and can be summarized as follows:

$$\nabla z : 1 - \lambda_0 \cdot e^T = r_z \tag{2.40}$$

$$\nabla \theta : \sum_0 \cdot \mathbf{g} + 2 \cdot \sum_\Omega \lambda \cdot \mathbf{L} \cdot \theta = r_\theta \tag{2.41}$$

$$\nabla \lambda_0 : f - z \cdot e^T + s_0 = r_{\lambda_0} \tag{2.42}$$

$$\nabla s_0 : \lambda_0 - \frac{\mu}{s_0} = r_{s_0} \tag{2.43}$$

$$\nabla \lambda_c : \theta^T \cdot \mathbf{L} \cdot \theta - |\Omega| \cdot {\varsigma_U}^2 + s_e \cdot |\Omega| = r_{\lambda_c} \tag{2.44}$$

$$\nabla s_c : \lambda_c \cdot |\Omega| - \frac{\Omega \cdot \mu}{s_c} = r_{s_c} \tag{2.45}$$

For the initial step homotopy facor μ is set to 0. This is updated in the subsequent steps of the predictor-corrector algorithm. For numerical stability the equations with respect to slack variables will be rewritten as follows by multiplying it by slack variables:

$$\begin{aligned} \nabla s_0 : \lambda_0 \cdot s_0 - \mu = 0 \\ \nabla s_c : \lambda_c \cdot |\Omega| \cdot s_c - \Omega \cdot \mu = 0 \end{aligned} \tag{2.46}$$

To exploit the sparsity which helps to reduce the computational effort, representation of the optimality condition can be written in matrix form. After linearising and using Schür complement the equation becomes the following (Eq. (2.47))which is solved towards updating the predictor step.

$$\begin{pmatrix} \lambda_0 \cdot \mathbf{H} + 2 \cdot \lambda_e \cdot \mathbf{L} & \mathbf{g} & 2 \cdot \mathbf{L} \cdot \theta & 0 \\ \mathbf{g}^2 & -\frac{s_0}{\lambda_0} & 0 & -e^T \\ 2 \cdot \mathbf{L}\theta^T & 0 & -\frac{s_c \cdot \Omega}{\lambda_c} & 0 \\ 0 & -e & 0 & 0 \end{pmatrix} \cdot \begin{pmatrix} \nabla \theta \\ \nabla \lambda_0 \\ \nabla \lambda_c \\ \nabla z \end{pmatrix} = \begin{pmatrix} r_\theta \\ r_{\lambda_0} \\ r_{\lambda_c} \\ r_z \end{pmatrix} \tag{2.47}$$

The results from the above step will be used to update the homotopy factor. Duality gap denoted by **dg** is computed to update μ.

$$dg = (s_0)^P \cdot (\lambda_0)^P + (s_c)^{P^T} \cdot {\lambda_c}^P \tag{2.48}$$

$$\mu = \beta \cdot dg \tag{2.49}$$

The solution from the predictor step is written with a superscript P as shown in equation 2.48. Using the updated μ the right hand side of the Eq. (2.47) is updated and it is solved again which is the corrected step. After this solution step a completer Predictor-Corrector iteration is completed for the sub problem. All the variables are updated after this step and the process will be continued until there is convergence.

2.4.2 Damping function

As mentioned before, one of the important criteria is to maintain the convexity of function, which helps in converging towards a global optimum. To make the optimization globally convergent every iteration has to be improvement. A method has been suggested by Svanberg et.al [23] which predicts conservative approximations to guarantee improvement in every iteration.

$$f^{(1)} = \hat{f^{(1)}} + \zeta^{(1)} \cdot d^{(1)} \tag{2.50}$$

Here $\hat{f^{(1)}}$ is original approximation, a conservative approximation is found by adding the damping function $d^{(1)}$ scaled by value called damping factor $\zeta^{(1)}$. A similar conservative approximation has to be made for the level two case also. The formulation of damping function is taken from the work of [20] which is stated below.

For the level one function the damping can be formulated as follows:

$$d^{(1)} = \sum_{n-n_c} (\mathbf{A_n} : {\mathbf{A_{n_0}}}^{-1} + \mathbf{D_n} : {\mathbf{D_{n_0}}}^{-1} + {\mathbf{A_n}}^{-1} : \mathbf{A_{n_0}} + {\mathbf{D_n}}^{-1} : \mathbf{D_{n_0}} - 12 \cdot \frac{\sum_{i=1}^{n-n_c} A_i}{\sum_{i=1}^{n} A_i}) \tag{2.51}$$

here the subscript 0 represents the value of the stiffness matrices at the approximation point. As done for function approximation in section 2.4.1, the damping function is calculated for the optimized nodes only therefore the summation of the nodes ranges from 1 to $n - n_c$. Similarly for the level two the damping function will take the following form:

$$d^{(2)} = \frac{1}{2} \nabla\theta^T \cdot \mathbf{H_d} \cdot \nabla\theta \tag{2.52}$$

in the above expression $\mathbf{H_d}$ is a regularization matrix that will be added to the $\mathbf{H}$ the hessian from level two approximation (in equation 2.30). The regularisation matrix is given as follows:

$$\frac{1}{s^2} \cdot \begin{pmatrix} 1 & -1 & & & & \\ -1 & 2 & -1 & & & \\ & \ddots & \ddots & \ddots & & \\ & & \ddots & \ddots & \ddots & \\ & & & -1 & 2 & -1 \\ & & & & -1 & 1 \end{pmatrix} + \begin{pmatrix} 1 & \dots & & & & 1 \\ \vdots & & & & & \vdots \\ & & \ddots & & & \\ & & & \ddots & & \\ & & & & & \vdots \\ 1 & \dots & & & & 1 \end{pmatrix} \tag{2.53}$$

At the approximation point the Scaling factor ζ is given the following,

initial scaling factor level one:

$$\zeta^{(1)^2} = \sum_{i}^{n-n_c} \frac{w_n}{2} \cdot ((\|\phi_m : \mathbf{A}^{-1} + \psi_m : \mathbf{A}\|)^2 + (\|\phi_b : \mathbf{D}^{-1} + \psi_b : \mathbf{D}\|)^2) \tag{2.54}$$

where w is a weighting factor given by

$$w_i = \frac{A_i}{\sum_i^{n-n_c} A_i} \tag{2.55}$$

initial scaling factor level two:

$$\zeta^{(2)^2} = \frac{1}{2} \cdot \mathbf{g}^T \cdot \mathbf{H_d}^{-1} \cdot \mathbf{g} \tag{2.56}$$

After setting the initial value, the damping function has to be updated to account for the change after each iteration. The update of the damping is done by checking the conservativeness of the new approximation using newly found point(x^*). Conservativeness is given by the following ratio between exact function f and its approximation $\hat{f}$

$$\zeta^* = e^{\frac{f(x^*)-f(\hat{x^*})}{d}} \tag{2.57}$$

$$\zeta^{new} = \zeta \cdot \zeta^* \tag{2.58}$$

To make sure that the damped approximation values calculated using Eq. (2.50) are not oscillating too much from the original approximations certain limits has to be applied to damping factor ζ. The rule applied to limit ζ given in the work of IJsselmuiden [20] is explained here. If the value of ζ^* is within 2 and 0.5 , then ζ^* is used for updating ζ using the equation 2.58. However if ζ^* exceeds the maximum limit of 2 or minimum limit of 0.5, the value is set to 2 or 0.5 respectively. Also a minimum of 1.05 is recommended by the author [20] if the value of ζ^* is between $1 - 1.05$. These limits helps to avoid large oscillation in optimization that can be caused due to non-conservative functions.

2.4.3 Fiber Path creation

Fiber angle distribution found from the optimization needs to be converted to fiber paths inorder to manufacture it using automated methods. Tows are parameterized such that it has distinct starting and end point and follows the angle distribution. This often creates gaps and overlaps in designs when two adjacent tows cross over each other. These are potential points that create stress concentrations in the structure. A.W Blom [18] proposes parameterizing the paths using streamline functions. These functions represent smooth streamlines optimized to reduce the thickness build up and follow the given distribution. The stream functions proposed by the author can be stated as follows:

$$\Psi(x, y) = \int_0^x t(x^*, y^*) \sin\theta(x^*, y^*) dx^* + \int_0^x t(x^*, y^*) \cos\theta(x^*, y^*) dy^* \tag{2.59}$$

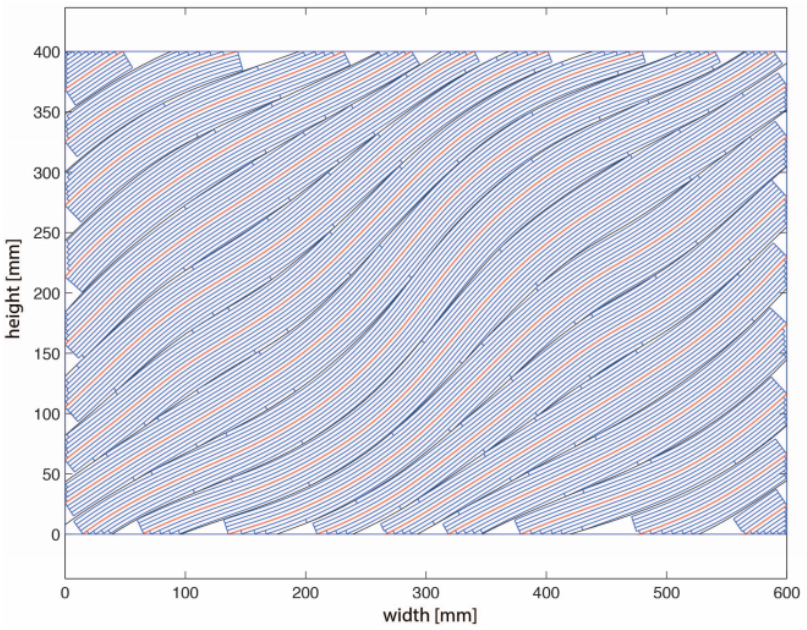

Figure 2.2: Tow drop effects in a steered fiber laminate [1]

For derivations of stream functions interested readers are referred to authors PhD thesis [18]. The above function is constructed terms of thickness t and the fiber angles θ which helps to create smooth thickness distribution. The tow drop effects in the steered laminates is presented in [1], which is shown below in figure 2.2.

In figure 2.2 the start and end point used for the tows are bottom and left edges & top and right edges respectively. These are also called inflow and outflow region. The selection of inflow and outflow regions does effect the fiber path pattern and tow drop effects. Although this task is not complicated for the rectangular plate shown in figure 2.2, depending on complexity of the structure it will not be a trivial task. Additional posit-processing would be required to judge the suitability of the fiber paths and inflow-outflow boundaries.

2.5 Manufacturing of Variable Stiffness laminates

2.5.1 Automated Fiber Placement

AFP technique was derived from Automatic tape laying(ATL). The earliest ATL machines made use of the existing Computer Numeric Control(CNC) knowledge to lay down tapes on a flat base plate [24]. The design from Goldsworthy in 1974 showed improved ability to lay tapes following a geodesic path on a curved surface. The machine consisted of fiber feeding head and compaction roller that held the material on the surface [25]. Most of the designs developed in late 70's were centered around aerospace application and therefore machines were custom built for aerospace specific part. Commercial machines were only introduced in 1980s after achieving considerable improvement in speed and ability to lay tapes on curved surface. Early efforts in 70's recorded productivity of 10-20 m/min(3-10 lb/hr) [7] which was considered inadequate to replace manual layup (2.5lb/hr).

Torres Martinez designed an automatic system for splicing(joining) tapes together which improved productivity by reduced downtime required for material refill [26]. By automating the

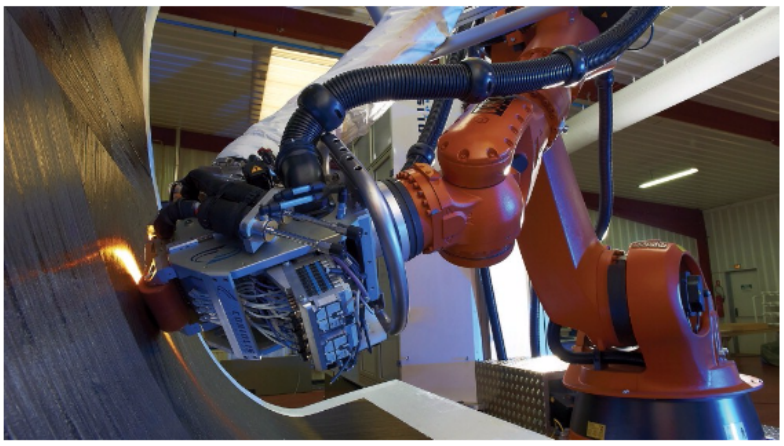

Figure 2.3: Modern multi-axial AFP machine
[7]

splicing of tapes they not only improved the productivity but reduced the chances of non-uniformity in tape end and errors in tape cutting making process more reliable. Similarly several improvements in capability of the AFP machines were achieved during the early 2000's which included infrared heating of tapes for better tack, off line programming and dual head systems for increasing productivity [27] [28]. The need of controlling the temperature and pressure was more evident with thermoplastic tapes as change in inter-facial heating and consolidation pressure had direct influence on the development of voids and layup quality [29].

Although considerable improvements were made in capability of the machines during the coming years, layup on curved and complex geometry is still an area requiring improvement. The improved modern machines can reach upto layup speed of 60 m/min which makes the fabrication of large structures realistic. However the involvement of fiber placement machines in automotive industry was fairly low, mainly due to small size and complexity of the automotive parts (which might result in generation of scrap material) and expense of the machine and raw material cost that are higher than resin transfer molded parts.

Influence of Manufacturing parameters

Although a fiber placement machine can be used to lay down curvilinear fibers, there are intrinsic problems in the manufacturing method that limits the possibilities that were proven theoretically. Main geometric factor that constraints how a curve should be is its radius of curvature. From a better design point of view, a machine that can lay down fibers with smallest radius of curvature should be the best one. But this factor is controlled by material stiffness, desired production speed and tow width. Variations in these manufacturing constraints and presence of process induced defects can change the buckling and in-plane response of the laminates from as low as 3% for flat parts to 40% for complex parts as shown in studies done by Pasini et.al [17] and Blom [18]. Similarly processing conditions such as temperature, compaction pressure, hold time also have influence on the fiber wetting or possibility of delamination which at the end effects part quality. Some of the influencing factors are discussed in the following section.

Effect of Tow width The effect of tow width is an important factor that decides the final strength of the design. Owing to the curvilinearity of the design, the fibers will have to be terminated at the points where the courses converge. Tow drops made at these points will leave

gaps in the design, which is an unavoidable aspect of AFP process. The effect of gaps and overlaps has to be accounted in the design stage. Narrow tows(3.175 mm, 6.35 mm) are used on small or complex shapes to reproduce the exact design. Wider tows (12.7 mm)are better suited for flat parts with limited steering especially wind turbine blades and aircraft wing skin.

Pasini et. al [17] performed numerical calculations for the effects of embedded defects in flat rectangular plate (10x16 in.) with constant fiber curvature design under uniaxial tension. For the comparison of the effect of tape widths the total width was always kept constant to 101.5 mm. Tape of width 12.7 mm resulted in 10% gap area which led to 10-12% reduction in buckling and in-plane strength. The performance was improved when a width of 3.175 mm was used which reduced gap area to 3-4%. The reduction in buckling and in-plane strength also came down to 3-4%. Results conforms the fact that dropping a wider tow will result in formation of larger gap as compared to narrow tow.

It should be noted here that number of tow drops incidents will be higher in the latter case which is discussed in the coming section. Percentage of gap area also depends on the part and complexity of fiber path distribution. Therefore the 10% reduction may become admissible as often cost of material and production speed have a say in deciding the tow width. For high performance application such as aerospace, tow width is a detrimental factor and often smallest tow width is preferred.

Effect of number of tows and steering radius AFP machine head can lay down 8 to 32 series of tows forming a course simultaneously at different speed and steering rate which allows more freedom and versatility. It has been shown that increasing the number of tows in a course can reduce the gap area %. This is mostly because of the reduced number of course boundaries which helps to reduce the need of tow drops and also the reduction in tow width(which helps in better steering). But using wider tows restricts the fiber steering ability as the radius of steering decreases with the width of the tow. This will influence the final strength of the laminate. The steering control or minimum steering radius is therefore a detrimental factor that should be considered during design stage.

Pasini et. al [17] studied the effect of number of tows on the gaps and overlaps and calculated the change in in-plane stiffness and buckling strength. A constant tow thickness of 3.175 mm was used and the number of tows was varied to check the behaviour of laminate with total gap, total overlap and no gaps and overlaps. The course with 8 tows resulted in gap area of 10.1% as compared to the course with 32 tows which only created gap area of 3.6%. Therefore increasing number of tows and using a smaller tow width can result in better design. Here a constant steering radius of 0.635m was assumed and it was shown that certain angle combination do not satisfy the steering radius constraint and are not manufacturable.

An optimization technique based on steering radius constraint have been proposed by Peeters et.al [9]. The result showed increasing steering radius does increase the buckling load of the laminate. The manufacturing constraint is then imposed on the design calculations to optimize the layups to obtain manufacturable designs. The fiber angles are then found out that satisfies the minimum steering radius constrain and curved paths are recovered. This means that not all layup designs can be manufactured and only the one's satisfying the constraints can be manufactured which was also shown by Pasini et.al [17]. This technique helps to include the effect of steering constraint in the design phase and therefore is very useful in this particular thesis.

Productivity

The productivity of the AFP machines have advanced with time. The most modern machines offer higher placement speeds upto 60 m/min [30]. There are lot of commercial machines available that can achieve this value, but the speed estimated is purely theoretical and difficult to realize in a real production scenario. The production speed is influenced by lot of parameters such as selected tow width, number of tows in a course and contour complexity therefore the real estimate of the speed cannot be predicted as it varies with each case.

Estimations of productivity was made for flat rectangular panel by Lukaszewicz et. al [31] which gives a general idea of speed of process that can be used for comparison with other fiber placement methods. The study involved benchmarking of AFP and ATL machine to compare the whole production routine. A 16m x 8 m flat plate made of 8 layers was considered for the study, the results are shown in the figure 2.4. Although the part size is more suitable for aerospace standards the benchmarking results are scalable and can be used as basis of comparison for smaller automotive part sizes too.

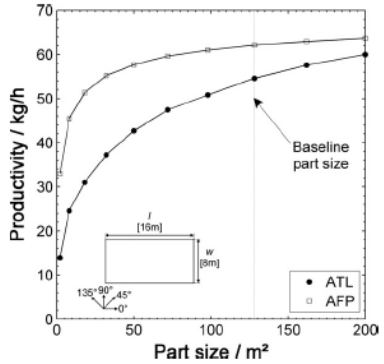

Figure 2.4: Productivity with respect to Part size

[31]

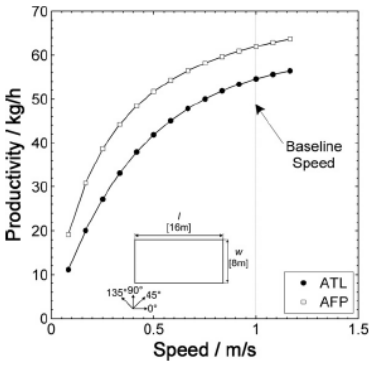

Figure 2.5: Productivity with respect to speed of process

[31]

Process	Part size (1m x 1m)	Part size (2m x 2m)
AFP	30.2 kg/h	41.4 kg/h
ATL	11.7 kg/h	29.2 kg/h

Table 2.1: Production speed comparison of AFP and ATL

As shown in figure 2.4, AFP and ATL shows linear increase in productivity with respect to part size and gradually reaches a plateau where the growths flattens out. The estimated theoretical prediction for both ATL and AFP method for a 1m x 1m flat plate and a 2m x 2m flat plate shown in table 2.1 proves that AFP gave a better production rate of 41.3 kg/h compared to ATL's 29.2 kg/h. But these rates will decrease very much when a real estimation is made. The main reason is intermittent acceleration and deceleration of the machine due to complexity of the part which result in creating secondary production time. This has been shown by Boeing whose theoretical estimate reached 45.4 kg/h but the real rate came down to 8.6 kg/h which shows that it is difficult to achieve high deposition rates as mentioned by Lukaszewicz [31]. The designs with higher percentage of short fiber course will result in creation of secondary

operation time in the form of time for cutting a new course, repositioning it and acceleration and deceleration accompanied with it. This is particularly important to take into consideration for this thesis as the structure to be produced is small as compared to aerospace structures.

Scaling the values of part size to comparable dimensions in automotive sector helps to assess the achievable production rates. Common automotive part size are below 2m x 2m which makes the production speed lower than large aerospace grade structures. Therefore the table of comparison 2.1 drawn from the results of Lukaszewicz [31] should show the representative production speeds for the automotive parts. The intermittent acceleration and deceleration will be an important factor for small and complex parts. Therefore it will be necessary to redesign parts to smoother shapes that can be economically produced using AFP method.

Material

Thermoset and Thermoplastic are the commonly used material system for automated layup process. The material is fed in the form of slit tapes into the machine head which then deposits it on the tool or mandrel with individual steering control. For AFP method slitting of the tape is an extra step in raw material processing, it is necessary since the fiber steering capabilities increase as the width of tape decreases. This extra step, together with the cost of manufacturing prepreg tapes results in high raw material cost.

Thermoset are more widely used with lot of previous knowledge about the mechanical properties. Most of the high-performance application prefer the material attributes such as aerial weight, ply thickness, modulus etc. to be tailored for the application. The recent trends in composite manufacturing shows demand for application specific materials being preferred in the industry [32]. Thermoplastics have been gaining importance due to the better impact properties, toughness and higher working temperature [33]. Thermoplastics have found application in aerospace and automobile sector for their superior properties, and ability to in-situ process and out of autoclave production makes it more attractive. This makes the bulking up of sections or joining of skin and stiffeners easier and certifiable. Although the thermoplastic fiber placement is energy intensive from the fact that it requires higher pressure and temperature as compared to regular thermoset fibers. This ofcourse has implications on the cost and complexity of the machine. Heating of the tapes needs to controlled to avoid developing residual stresses and these are often done by state of the art laser or infra-red heating methods.

Dry fiber placement methods have also gained interest due to its possibility to make use of uncured material (therefore longer process time) which makes it possible to make large and complex integrated structures. The drawback is that low stiffness nature of the dry fibers requires careful deposition to achieve required fiber angle and the fiber architecture needs to optimized for the resin infusion step [11]. This method is lot similar to the TFP although TFP machines can produced highly steered designs compared to that of fiber placement machines.

Cost

The cost of AFP machines is a decisive factor in adopting this method. AFP machines are expensive compared to other fiber placement methods especially TFP. The initial investment required for these machines often restricts its usage to high production rate process or high performance applications. Modern AFP machines can range from $1-6 million [7]. The gantry type machines that are typically used for manufacturing large parts costs around $4-6million. The smaller modular robotic systems can be cheaper $1-2 million [31]. For automotive application usually smaller robotic systems are an affordable option which can effectively handle small

parts with replaceable modular heads. Offsetting the initial investment can take time depending on the industry which creates additional risks. Although cost is a contradicting factor, other benefits such as reproducibility, reduced material wastage and ability to produce complex fiber architecture outweigh those disadvantages especially when it comes to high tech application.

2.5.2 Tailored Fiber Placement

Textile production techniques were well known even before the introduction of TFP machines. The stitching technique that was already existing to manufacture clothes were translated to structural designing by replacing thin threads with reinforcing fibers. Lots of researches were carried out in IPF Dresden in 90's, and is often accredited as first to introduce this techniques in composite structural designing [34] [35] [36]. The method is still a growing field and lot of research and development is going on to better understand and model the effect of different stitching techniques.

Influence of Manufacturing parameters

TFP head can lay down dry fiber yarns in practically any angle or curvature on the base material. The ability to achieve near net shaped preforms with minimal wastage as compared to AFP makes it different from other fiber placement techniques. This gives the possibility to reproduce the bionic stress paths to near perfection, which is impossible to achieve with AFP machines.

Also a salient feature of the method is the use of stitching threads that runs through the thickness to tie the fibers in place. This offers the possibility to reinforce in z-direction which gives better out of plane performance. This feature gives laminate produced using TFP method better fracture toughness, interlaminar strength, impact, Compression after impact (CAI) performance which has been proven by Spickenheuer et.al [37]. Mattheij et.al [34] showed that using reinforcing fibers as stitching threads (3D stitching)brought significant improvement in Mode I fracture toughness and CAI strength. Use of reinforcing fibers for preform manufacturing improves the strength in out of plane direction which is particularly attractive for thick laminates and also one of the differentiating factor compared to AFP. But these advantages often come at the cost of in-plane properties as the needle paths are sources of resin rich areas. The challenge of current generation TFP methods are to improve the out-of plane performance while providing required in-plane properties and producing it in reasonable speed. The above specified requirements of the method depends on certain manufacturing parameters that are to be considered at design stage.

Effect of Stitching length & Stitching width In TFP the dry fibers are placed in position by stitching it to the base material. The stitching length or frequency is an important factor that determines the strength of the laminate. The stitching length influences the stiffness and strength of the laminate. A smaller stitching length or a higher frequency of stitching increases the stiffness of the laminate but often result in lower tensile strength. Stitching will create fiber waviness which alters the fiber angles within a course and this result in lower tensile strength. Spickenheuer et.al [37] showed this effect by experimental testing of UD tension specimen manufactured by TFP. The reduction in tensile strength is also because of the breakage of fibers during stitching which is visible in the test results of Spickenheuer. The results shows increase in tensile strength with increase in stitching length and inverse for stiffness.

Stitching width is the determining parameter that decides the amplitude of the waviness formed during preform manufacturing. Smaller widths are often preferred since it will restrict the movement and amplitude of the wave which improves the stiffness of the laminates. But as mentioned earlier the fiber breakage due to tighter stitching should be also taken into consideration while choosing stitching width. Varying the stitching density throughout the laminate to suit the strength and stiffness requirements can lead to better performance than using a uniform stitching density.

Apart from the stitching, using thicker dry fiber bundles for preforms can reduce the fiber waviness to an extent due to its increased sectional area. Thick layers are not preferred in conventional unstitched laminates due to interlaminar stress development between the layers. This issue can be answered by stitching layer together which generally offer better interlaminar strength than an unstitched laminate.

Productivity

The productivity of the TFP process is comparatively much lower than that of the AFP method. The production speed of a TFP machines are depended on the governing parameter such as stitching density, fiber yarn size and fiber steering. A single head TFP machine can produce 1kg/hr at a linear speed of 10m/min [38], these rates are benchmark for structure with less complexity and using a 50K(50,000 filaments in fiber tow) tow fiber, but the realistic rate comes down to 3m-5m/min.

Process	Part size (1m x 1m)	Part size (2m x 2m)
AFP	30.2 kg/h	41.4 kg/h
TFP	1 kg/h	1 kg/h

Table 2.2: Production Speed Comparison

Since the TFP ,machine can deposit 12K tow and a 50K tow at almost same speed it is rewarding to use thicker tows to increase the production rate. The production rate of 12K tow comes down to 0.3kg/hr which is considerably lower than that of 50K tow. Since the methodology of TFP is to stitch dry fiber tows on preforms one after other, it will be only realistic to produce small parts considering the production time. But multiple head TFP machine can accommodate upto 30 heads that makes it suitable for large scale production purposes.

Practices such as selective stitching, deep drawing and smarter optimization of fiber paths and stitching density can save production time and result in parts better than conventional laminate design. Famous example of TFP produced aerospace part is carbon fiber window frame for Airbus A350 which resulted in design that is almost stress concentration free [38]. This was achieved through selective stitching and structural stitching and further stretching the preforms to shape. TFP has also found potential application in automotive sector, where crash cones, chassis and suspension parts are being manufactured using the method.

Material

The most common material form used for TFP preform is dry fiber tows. All type of reinforcing fibers such as carbon, glass and aramid can be used for preform manufacturing. Resin system

is usually transferred into the stitched preform through liquid molding processes such as Resin Transfer molding or Vacuum infusion. There is a variety of sewing threads available for stitching, depending on the purpose it can be thin polyester yarns of 5 tex to aramid fibers of 40 tex. In both the cases the compatibility of sewing threads with resin system is increased with application of sizing.

Lot of new material processing methods are being explored all over the world. One of the example is customized hybrid fiber development technique 'SPINCom' from Leibniz Institute Dresden [39], uses simultaneous melt spinning polymer (thermoplastic) and fiber and in-situ commingling offered highly homogeneous material. Such materials can play important role in providing uniform fiber volume content which is difficult to achieve with Liquid molding process. TFP made parts are prone to resin rich areas therefore there is high importance for hybrid materials.

Cost

Cost of the TFP machine is one of the high points in comparison to its other counterparts. A multiple head (usually $8-10$ heads, can go upto 30 heads) TFP machine can be installed at $\$300,000$ which is only fraction of what a AFP machine costs [38]. The low initial capital together with cheaper raw material expenses makes it very good option for manufacturing steered fiber reinforced structures. Although the productivity of the machine is quite low, using multiple machine can result in productivity close to that of AFP machines.Using four TFP machines 10 heads each will help to scale the production process and cost of the machines will be equal to that of a AFP machine as shown in the Table 2.3.

Process	1xTFP	4xTFP	AFP
Speed	1-10 kg/h	1-40 kg/h	41.4 kg/hr
Cost	$300,000	$1,200,000	>$1,200,000

Table 2.3: Cost Comparison

However stitching is an additional step in laminate fabrication which will be followed by resin transfer that additionally requires part specific molds and autoclaves. These can be considered as non-recurring expense similar to machine cost. Overall cost TFP method would be still much more attractive than AFP method owing to cheaper machines and raw material.

2.6 Conclusion

An overview of the design and manufacturing aspects of variable stiffness laminates was given in this chapter. The design optimization method presented here is based on the previous research and development done in TU Delft. An interior point method is used for optimizing the fiber angle distribution at nodal points by formulating a convex function at each node [1]. The functions represent outcome of the FEA that are essentially structural responses. These responses are obtained by performing a 2D finite element analysis. Along with the responses, the sensitivities are calculated as well, these are further used for creating approximations. Structural approximations are used in the multi-level optimization approach where more than one optimization function is used for efficiency. For the optimization method presented here two level of

approximations are created namely level one and level two. The method of multiple approximations has shown computational efficiency [1] [23] as it helps to reduce number of FEA's during the optimization. The end result of the optimization is optimized fiber angle distribution that are manufacturable. Fiber paths are created from this distribution by curve fitting these angles to a streamline function [18].

For manufacturing variable stiffness laminates, Fiber placement techniques are instrumental in exploring benefits offered by high anisotropy of composite materials. Both the manufacturing methods assessed in the study are different in their own way. Automated Fiber placement technique is very well suited for manufacturing large structures such as wing or fuselage section due to its high production rate. The fiber steering capability of the machine is limited in comparison to the TFP method but still shows significant improvement in terms of weight and strength as compared to the conventional UD laminates [10]. The main area of concern will be the reduction of gaps or overlaps caused due to tow drops. These are essentially areas that causes stress concentrations which are undesirable in a structure. Also the high initial expense for the machines and energy requirements for curing or consolidation (depending on whether the material is thermoset or thermoplastic) limits its usage to high performance application.

TFP made parts generally show better out of plane properties, this is one of distinguishing facts compared to AFP made parts. Especially use of 3D stitching shows significant improvement in impact performance and delamination resistance which makes it suitable for manufacturing crashworthy structures. But low productivity rates are the main drawback of the method which restricts it usage in fabrication of large structures. A trade-off table comparing their features are presented in Table 2.4.

Parameter	AFP	TFP
Preform Production time (Part size: 1m x 1m)	1.6 min @ 20.02 kg/hr	24 min @ 1 kg/hr
Preform Production time (Part size: 2m x 2m)	2.3 min @41.34 kg/hr	48 min @ 1 kg/hr
Real production rate	8.6-10 kg/h	0.5 kg/h
Cost	$1,200,000	$300,000
Mass production rate	41.34 kg/hr	40 kg/hr @ using 40-stitching head
Effect of defects on stiffness and strength	3-10%	5-16%
Scrap generation	5-7 %	0-1%
Suitable parts	roofs, body floor, drive shafts	crash cone, chassis parts, suspension parts, drive shafts

Table 2.4: Trade-off Table

Both methods allow production of variable stiffness composites with significant improvement from UD laminates. The deciding factor can therefore be cost and complexity of structure. It can be concluded with some assertion that TFP method would be preferred when the part is small to medium sized $(1 - 10m^2)$ and if loading condition is dominated by out of plane loads. TFP is particularly suitable for automotive production due to its scalability to meet high production rates. Although the process induced defects tends to be high for TFP, desired

fibre volume content of automobile parts are around 50%-60% which is quite achievable with TFP-RTM combination. The ability of the method to make near net shaped preforms helps to reduce need of further machining. TFP also allows to design tailored preforms for the placement of inserts without additional machining. Curing of resin with inserts in place helps to further strengthen structural joint between insert and preform. The automotive parts requiring high impact resistance such as bumpers, crash structures would be ideal targets for TFP.

AFP method will be more suitable when the structure is medium to large sized ($10 - 100m^2$) (see Figure 2.5) and when higher production rate is to be attained. The production rates for structures smaller than $1m^2$ (typical automotive parts size) will be lower than 30 kg/hr. Also the steering constraints in AFP machines will make steering of fibers on highly complex parts such as chassis and suspension difficult. Material-wise, use of tape material offer better control and finish quality but at higher cost. Since raw material costs are recurring it is not a desirable method for low-end commercial applications.

In comparison it can be concluded that TFP can be cost-effective method for automobile composite structure manufacturing. With the use of advanced material and processing methods the quality can be raised to comparable standards of AFP method. Upcoming technologies such as High-Pressure Resin Transfer Molding together with short cure cycle resins, makes the use of TFP method much more attractive and affordable for automotive application.

Chapter 3

Model Setup

The model used for the thesis is part of an automotive structure. The part studied in this thesis is shown in Figure 3.1. It consists of an outer shell reinforced inside with cores and rib-like structures. The outer shell is made out of composite material. The composite shell that is optimized will be called "Main Shell" from here on and the inner parts are divided into: baffle core (which is made of isotropic material) , baffle shells (which is made of composite material). The baffle shell and the baffle core parts are not optimized however their influence is taken into consideration (i.e, the entire model is subjected to finite element analysis for calculating the responses). For the visibility of the inner parts an exploded view is shown in Figure 3.2 for further details.

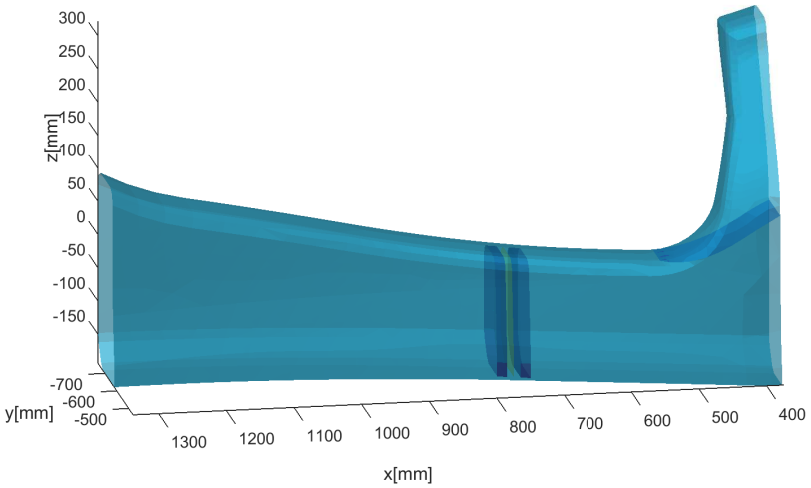

Figure 3.1: Model with positions of subparts visible

The material properties used to model these parts are summarized in the Table 5.4. Here $E1$ and $E2$ represents properties in 1 and 2 orthogonal directions respectively , μ represents poisson's ratio and G_{12} the shear modulus. Density of the material is given by ρ and the strength allowable in X direction in tension is given by X^t and in compression X^c. Similarly strength allowable in Y direction is given by Y^t in tension and Y^c in compression.

Property	Composite	Isotropic
E1,[MPa]	120000	85
E2,[MPa]	6500	85
μ_{12}	0.018	0.38
G_{12},[MPa]	3000	30.8
ρ,$[\frac{kg}{mm^3}]$	$1.78e^{-9}$	$9e^{-11}$
X^t,[MPa]	1800	-
X^c,[MPa]	900	-
Y^t,[MPa]	10000	-
Y^c,[MPa]	10000	-
S,[MPa]	10000	-

Table 3.2: Material Properties

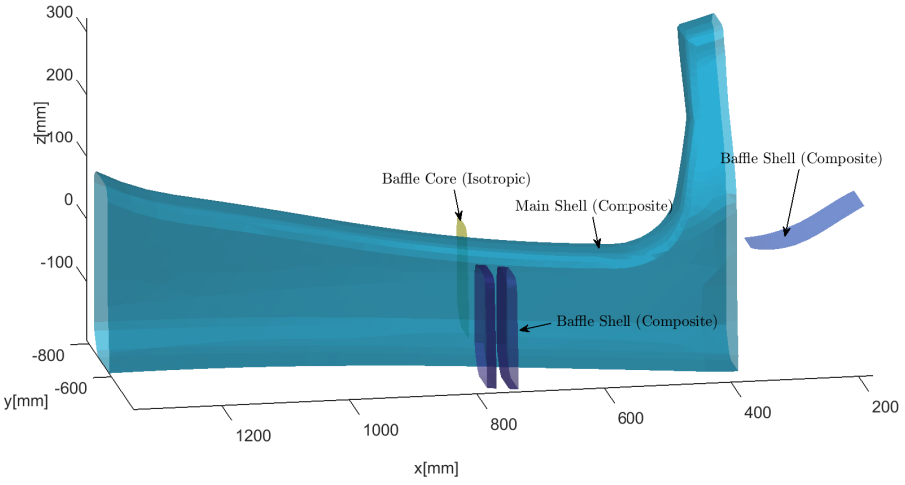

Figure 3.2: Exploded view of the model

3.1 Laminate Stacking Sequence

The layup and thickness distribution is obtained from the model(provided by DES Composites) created in Altair Hyperworks. It should be noted here that the model provided for this thesis has already undergone an optimization using Altair Hyperworks Optistruct. The resulting laminate and thickness distribution is used as initial design or starting point for the optimization problem. This will help to understand if the variable stiffness laminate designs can be beneficial compared to an optimized conventional laminate design (or Uni-directional ply based design). The sub laminates present in the model and their layups are shown in the table 3.3.

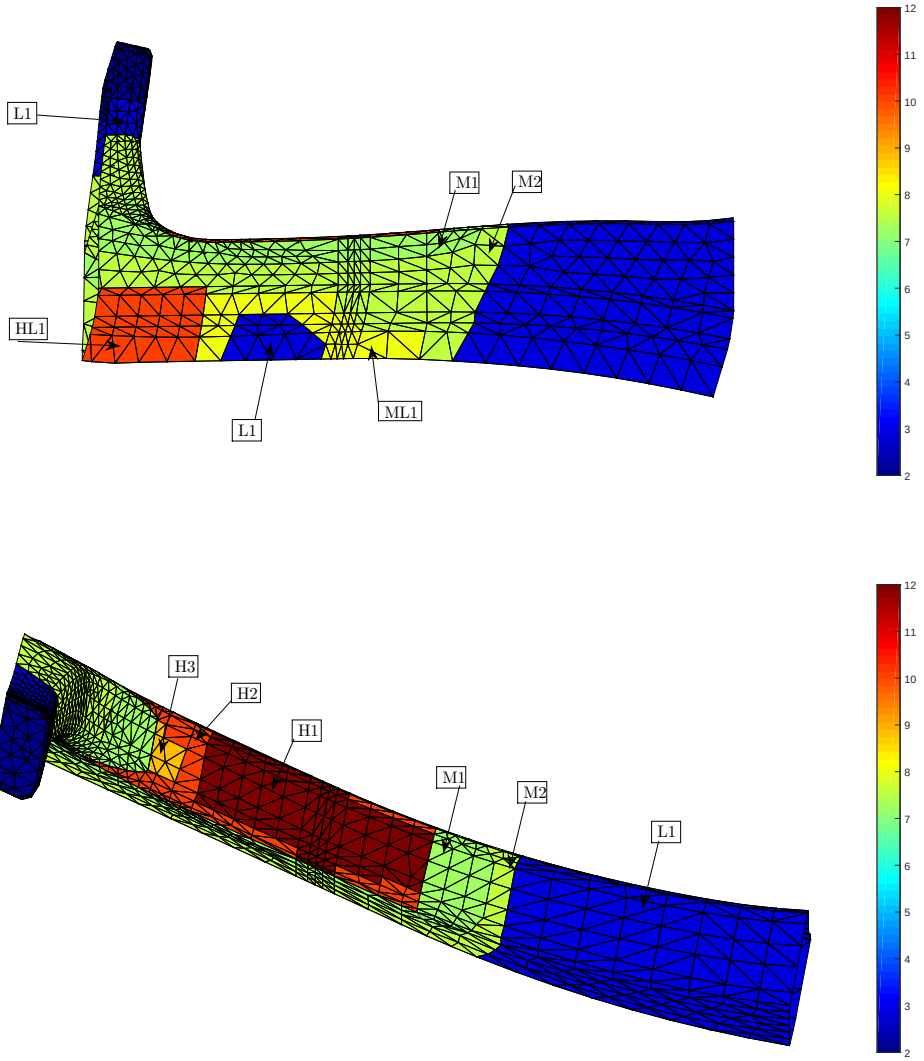

Figure 3.3: Laminate codes and thickness distribution in [mm]

The thickness build up of the model in figure 3.3 has laminate codes (such as 'M1' or 'M2') which corresponds to a specific stacking sequence which is shown in the table 3.3.

It can be seen that the number of layer are quite high which does have a influence in computation since the number of design variables increases. The sizes of the matrices used in optimization are in terms of number of nodes X number of layers. This was seen to effect the memory usage

Laminates	Layups
H1	$[45_2/90_2/0_2/45/90_2/0_2/45/90_2/0_2/45/0_2/45/0_4]_s$
H2	$[45_2/0_2/45/90_2/0_2/45/0_2/45/0_2]_s$
H3	$[45_2/0_2/45/90_2/0_2/45/45]_s$
M1	$[45_2/90_2/0_2/45/90_2/45/45]_s$
M2	$[45_2/0_2/45/90_2/45/0_2]_s$
L1	$[45_2/90_2/0_2/45]_s$
HL1	$[45_2/0_2/45/0_8]_s$
ML1	$[45_2/90_2/0_2/45/0_4]_s$

Table 3.3: Stacking Sequence of the model

during optimization. Therefore initial layup has been changed by doubling the thickness and decreasing the number of layers. To maintain the validity of the design optimization problem the comparison of the improvement will be done with respect to the modified layup instead of the parent layup shown in Table 3.3. The modified layup used for the optimization is shown in Table 3.4.

Laminates	Layups
H1	$[45_2/0/45/90/0/45/0/45/0]$
H2	$[45_2/0/45/90/0/45/0/45/0]$
H3	$[45_2/0/45/90/0/45/45]$
M1	$[45_2/0/45/90/45/45]$
M2	$[45_2/0/45/90/45]$
L1	$[45_2/90/45]$
HL1	$[45_2/0/45/0_3]$
ML1	$[45_2/90/0/45/0_2]$

Table 3.4: Modified Design layup

Interpretation of the design layup : For the optimization , balanced and symmetric condition are used. The layup given above is the design layers that are optimized. The balanced and symmetric layers will be taken into account during FEM analysis. Therefore a design layup of $[\theta_1/\theta_2 \dots]$ should be interpreted as $[\theta_1/-\theta_1/\theta_2/-\theta_2 \dots]_{sym}$. This is applied to the modified design layup shown in the Table 3.4 for the DES model.

3.2 Meshing of the Model

The model is created in Altair HyperWorks Optistruct software which is capable of FEM analysis and optimization. Meshing will be done with triangular elements since the optimizer is based on triangular elements. These triangular elements are later turned into higher order triangular elements by formulation(see chapter 4). The model is meshed keeping in mind the computational effort that is to come later on in the optimization. The optimization problem is setup with objectives or constraints set per node (refer to chapter 5), therefore computational time scales up as number of nodes increases. A coarser mesh has been created using the automesh feature in Altair Hyperworks. Finer meshing was done only on the curved section, for accurately representing geometry and also to capture the stress variations. The curved region is strength critical region (see Section 4.3) therefore finer elements are biased to those region. Flat sides away from the curved regions are less critical and therefore coarser mesh is used there. There are partitions made on the structure to suit the laminate regions which can be seen from the Figure 3.3.

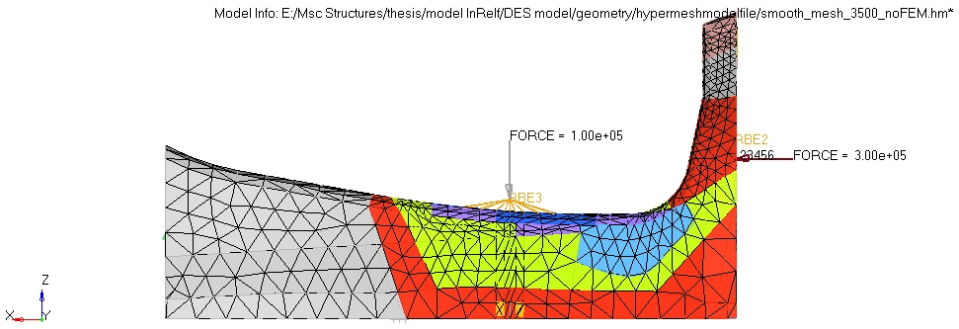

3.3 Boundary Conditions

There are two loadcases analyzed in this thesis, namely :

1. Bending Loadcase
2. Inertia Relief Loadcase

The bending loadcase is created with a load of $1e^5[N]$ acting along the z-axis of the model that causes the structure to bend around z axis. Fixed (or clamped, all 6 degrees of freedom) constraints are applied on the two ends of the model as shown below Figure **??**. The load is point load transferred to a set of points through MPC constraint. The formulation of MPC Constraints are given in the coming section 3.3.1.

The second loadcase, is the inertia relief loadcase. Here a force of $3e^5[N]$ is applied along the X-direction of the model on the edge of the model as shown Figure 3.5. The load is distributed to the nodes through a Rigid body element ($RBE2$). These elements take into account the kinematics of the master node (which is a fictitious node that doesn't add stiffness to structure). The formulation of a $RBE2$ element is given in section 3.3.2. For the inertia relief case the body is not constraint as it is considered as a rigid body. The inertial force acting on the body

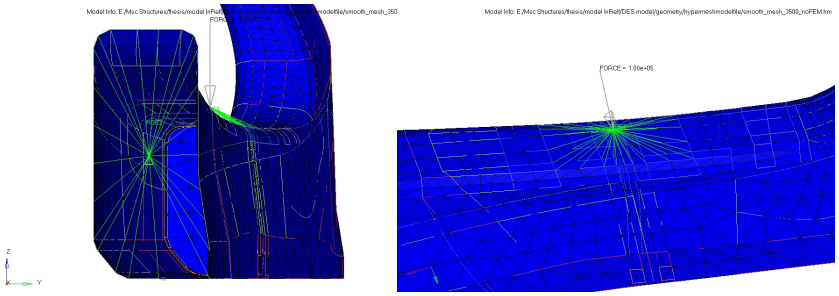

Figure 3.4: Boundary Condition for bending loadcase

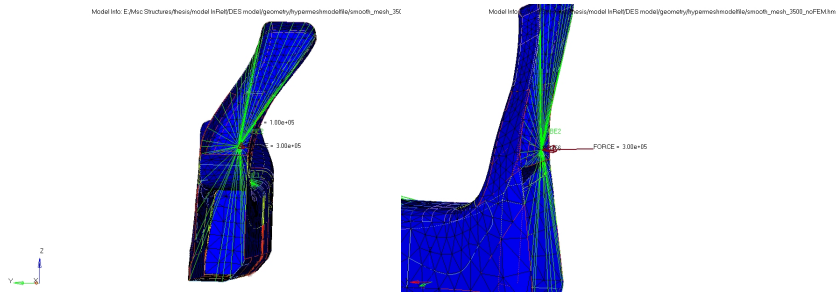

Figure 3.5: Boundary Condition for bending loadcase

Loadcase	Load [N]	Constraint
Bending	$1e^5$	clamped-clamped
Inertia Relief	$3e^5$	Free-Free

Table 3.5: Boundary Condition

is used to balance the applied load, and a static analysis is done. The formulation of inertia relief analysis is described in the chapter 4.

The responses of the two load cases will be used for optimization separately. The responses and its sensitivities will be calculated by performing 2 separate FEA's, which will then be used for formulating function (or the structural approximations explained in chapter).

3.3.1 Multi point constraints

Boundary Conditions can be framed in several ways to approximate the behaviour of the structure. When it comes to force boundary conditions, tie joints or kinematic joints are common in structures. Here a dependent node or nodes is influenced by a master node or set of master nodes. This influence can be expressed by using a predefined formula that would involve contributions of master nodes. The Multi-point constraint (MPC) relation can therefore be generalized as follows:

$$u = T \cdot \hat{u} \tag{3.1}$$

Here T which relates the slave degrees of freedom to master degree of freedom. When it comes to linear relations (usually in linear static analysis, where non-linearities are neglected) T would

be filled with integer numbers and zeros. This transformation matrix has to be applied to the stiffness matrix and force vector to get the modified system of equations.

$$\hat{K} = T^T \cdot K \cdot T \tag{3.2}$$

$$\hat{f} = T^T \cdot f \tag{3.3}$$

The modified system can be solved for getting the displacements of master and independent degrees of freedom.

$$\hat{K} \cdot \hat{u} = \hat{f} \tag{3.4}$$

After finding $\hat{u}$, the full displacement vector can be found out from the relation given in equation 3.1. This is the general method for solving MPC's , depending on the joint or constraint in context the T matrix has to be modified. In the given model a kinematic constraint in the form of $RBE2$ element is used. This is essentially a MPC constraint with additional consideration for kinematics of the joint. Formulation of $RBE2$ element is explained in the next section.

3.3.2 Rigid body elements (RBE2)

$RBE2$ elements takes into account both the translational degrees of freedom (DOFS) as well as rotational degrees of freedom. Therefore a slave node will be related to the master node by all the 6 DOFS. This means that translation of slave node is not just related to translation of the master node but also its rotation. The rotation or slave node is only depended on the rotation of master node. This relation can be summarized into the so called rigid-body transformation matrix as follows:

$$\begin{pmatrix} \tilde{u_{x_i}} \\ \tilde{u_{y_i}} \\ \tilde{u_{z_i}} \\ \tilde{u_{\theta_{x_i}}} \\ \tilde{u_{\theta_{y_i}}} \\ \tilde{u_{\theta_{z_i}}} \end{pmatrix} = \begin{pmatrix} 1 & 0 & 0 & 0 & \triangle(z) & -\triangle(y) \\ 0 & 1 & 0 & -\triangle(z) & 0 & \triangle(x) \\ 0 & 0 & 1 & \triangle(y) & -\triangle(x) & 0 \\ 0 & 0 & 0 & 1 & 0 & 0 \\ 0 & 0 & 0 & 0 & 1 & 0 \\ 0 & 0 & 0 & 0 & 0 & 1 \end{pmatrix} \cdot \begin{pmatrix} u_{x_j} \\ u_{y_j} \\ u_{z_j} \\ u_{\theta_{x_j}} \\ u_{\theta_{y_j}} \\ u_{\theta_{z_j}} \end{pmatrix} \tag{3.5}$$

Here u_i represents degrees of freedom of slave node and u_j degrees of freedom of master node. Similar relation can be created for all the required slave nodes as assembled together to form the transformation matrix T. After formulating T, the method shown in Section 3.3.1 can be followed.

Chapter 4

Finite Element Formulation & Inertia Relief

Inertia Relief is a method of structural analysis used for unconstrained bodies that experiences body forces and inertial forces that are generated by virtue of its motion [40]. A few examples of such structures are aircraft in flight, automotive body on a suspension and a spacecraft. If the example of aircraft is taken, wing of an aircraft deforms under the aerodynamic forces when in flight. But the acceleration of the aircraft also imposes the rigid body motion of the wing. These two modes when superimposed will result in the final state of the structure in real life. The more traditional cantilever type static analysis of a wing will therefore be inaccurate in predicting the state of the structure. For this thesis the structure in context is part of automotive body, which also undergoes similar unconstrained or partially unconstrained motion on a suspension. Therefore it is interesting to see the Inertia Relief load case applied on this structure. Although these type of structures can be analyzed with transient dynamic analysis methods [41] , they are often computationally expensive compared to Inertia Relief. It has been shown by Nelson and Wolf [42] that the structures with higher frequency loads can be effectively analyzed with inertia relief loads with good accuracy. Their study also showed that inertia relief analysis tends to be inaccurate in low frequency and resonance conditions.

4.1 Finite Element Formulation

The finite element formulation of structure is done by discretizing the domain into finite elements. A higher order triangular element [2] formulated by Carlos A. Felippa will be used throughout this thesis. As explained by the author Higher order elements are basically high performing simple elements(elements with corner nodes only) that can predict results with engineering accuracy with coarser mesh or reduced computational time. In the case of selected triangular element, an added drilling degrees of freedom 4.1to the nodes makes it much superior than constant strain elements.

The displacements of the structure is obtained by solving the equilibrium equation. The equilibrium equation solved in finite element analysis is derived from the assumption that change in potential energy is zero at state of equilibrium. This results in the familiar equation:

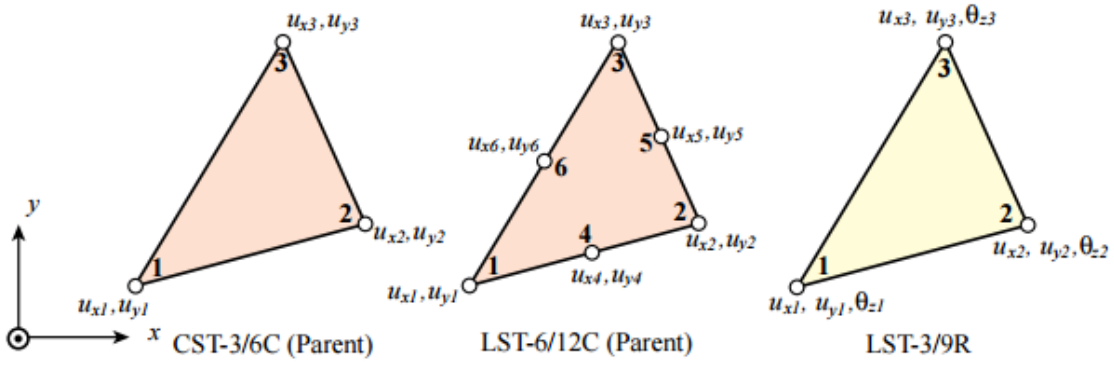

Figure 4.1: Higher Order Triangular Element [2]

$$[\mathbf{K}][\mathbf{U}] = [\mathbf{F}] \tag{4.1}$$

Here K is the stiffness matrix U is the displacement vector and F is applied force vector. The formulation of stiffness of higher order triangular element is given in the coming section which will be used throughout this thesis except for the inertia relief of beam presented in 4.2.1 where beam is modeled using $1D$ element.

4.1.1 Higher order Triangular Membrane Element

The displacement of nodes are assembled together in vector **U** together with the added drilling degrees of freedom which can be expressed as follows:

$$u = \begin{bmatrix} u_{x1} & u_{y1} & \theta_{z1} & u_{x2} & u_{y2} & \theta_{z2} & u_{x3} & u_{y3} & \theta_{z3} \end{bmatrix} \tag{4.2}$$

$$where, \theta_z = \frac{1}{2}\left(\frac{\partial u_y}{\partial x} - \frac{\partial u_x}{\partial y}\right) \tag{4.3}$$

The formulation of element is done in the neutral axis directions as shown in figure 4.2. Author uses a transformation matrix to convert the Cartesian system to newly defined direction. The strains are decomposed into natural strains and deviatoric strains for the formulation of stiffness matrix. The natural strains are measured along the 3 side directions that match the neutral axis of triangle. Natural strains ϵ can be expressed in terms of Cartesian strains e with help following transformation matrix

$$\begin{pmatrix} \epsilon_{12} \\ \epsilon_{23} \\ \epsilon_{31} \end{pmatrix} = \begin{pmatrix} {x_{21}}^2/{l_{21}}^2 & {y_{21}}^2/{l_{21}}^2 & x_{21}y_{21}/{l_{21}}^2 \\ {x_{32}}^2/{l_{32}}^2 & {y_{32}}^2/{l_{32}}^2 & y_{32}x_{32}/{l_{32}}^2 \\ {x_{13}}^2/{l_{13}}^2 & {y_{13}}^2/{l_{13}}^2 & y_{13}x_{13}/{l_{13}}^2 \end{pmatrix} \begin{pmatrix} e_{xx} \\ e_{yy} \\ e_{xy} \end{pmatrix} = {T_e}^{-1} e \tag{4.4}$$

Here the value (x_{ij}) is coordinate difference of nodes and l_{ij} can be written in terms of x_{ij} and y_{ij} as follows

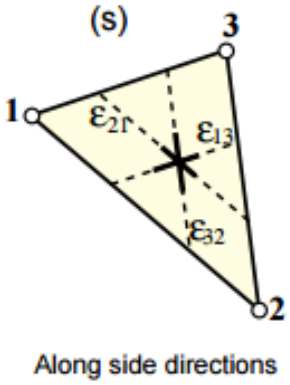

Figure 4.2: Natural Strain directions [2]

$$x_{ij} = x_i - x_j \tag{4.5}$$

$$y_{ij} = y_i - y_j \tag{4.6}$$

$$l_{ij} = \sqrt{{x_{ij}}^2 + {y_{ij}}^2} \tag{4.7}$$

The material stiffness matrix which is in the cartesian coordinate system can also be transformed using the above transformation matrix to natural coordinate system in the following way as shown below:

$$\mathbf{A_{m_{nat}}} = {\mathbf{T_e}}^T \cdot \mathbf{A_m} \cdot \mathbf{T_e} \tag{4.8}$$

The drilling rotation can be obtained by subtracting the constant strain triangle rotation $\theta_\mathbf{0}$ from the total corner rotation $\theta_\mathbf{i}$:

$$\tilde{\theta} = \theta_\mathbf{i} - \theta_\mathbf{0} \tag{4.9}$$

here $\theta_\mathbf{0}$ for the three corner nodes is given by

$$\theta_\mathbf{0} = \frac{1}{4A}(x_{23}u_{x1} + x_{31}u_{x2} + x_{12}u_{x3} + y_{23}u_{y1} + y_{31}u_{y2} + y_{12}u_{y3}) \tag{4.10}$$

Using the above relation displacements can be assembled as follows,

$$\begin{pmatrix} \tilde{\theta_1} \\ \tilde{\theta_2} \\ \tilde{\theta_3} \end{pmatrix} = \begin{pmatrix} \frac{x_{32}}{4A} & \frac{y_{32}}{4A} & 1 & \frac{x_{13}}{4A} & \frac{y_{13}}{4A} & 0 & \frac{x_{21}}{4A} & \frac{y_{21}}{4A} & 0 \\ \frac{x_{32}}{4A} & \frac{y_{32}}{4A} & 0 & \frac{x_{13}}{4A} & \frac{y_{13}}{4A} & 1 & \frac{x_{21}}{4A} & \frac{y_{21}}{4A} & 0 \\ \frac{x_{32}}{4A} & \frac{y_{32}}{4A} & 0 & \frac{x_{13}}{4A} & \frac{y_{13}}{4A} & 0 & \frac{x_{21}}{4A} & \frac{y_{21}}{4A} & 1 \end{pmatrix} \begin{pmatrix} u_{x1} \\ u_{y1} \\ \theta_1 \\ u_{x2} \\ u_{y2} \\ \theta_2 \\ u_{x3} \\ u_{y3} \\ \theta_3 \end{pmatrix} = \tilde{T_{\theta u}} u_R \tag{4.11}$$

The stiffness matrix is written as a combination of basic K_b and hierarchical stiffness K_h. The basic stiffness takes the form,

$$\mathbf{K_b} = \frac{\mathbf{L} \cdot \mathbf{A_m} \cdot \mathbf{L^T}}{\mathbf{A}} \tag{4.12}$$

in the above equation, Am is the membrane stiffness of the element(which is made of composite material). The membrane stiffness is integrated over the thickness as mentioned in chapter 2. And A represents area of the element. L is called force-lumping matrix, which is similar to strain displacement matrix B.

$$L = \frac{1}{2}\begin{Bmatrix} y_{23} & 0 & x_{23} \\ 0 & x_{23} & y_{23} \\ \frac{1}{6}\alpha_b y_{23}(y_{13}-y_{21}) & \frac{1}{6}\alpha_b x_{32}(x_{31}-x_{12}) & \frac{1}{3}\alpha_b(x_{31}y_{13}-x_{12}y_{21}) \\ y_{31} & 0 & x_{13} \\ 0 & x_{13} & y_{31} \\ \frac{1}{6}\alpha_b y_{31}(y_{21}-y_{32}) & \frac{1}{6}\alpha_b x_{13}(x_{12}-x_{23}) & \frac{1}{3}\alpha_b(x_{12}y_{21}-x_{23}y_{32}) \\ y_{12} & 0 & x_{21} \\ 0 & x_{21} & y_{12} \\ \frac{1}{6}\alpha_b y_{12}(y_{32}-y_{13}) & \frac{1}{6}\alpha_b x_{21}(x_{23}-x_{31}) & \frac{1}{3}\alpha_b(x_{23}y_{32}-x_{31}y_{13}) \end{Bmatrix} \tag{4.13}$$

For an optimal element the value of α_b is $\frac{3}{2}$ [2]. The hierarchical part of the stiffness is written in terms of drilling rotations $\tilde{\theta}$ and the transformation matrix explained in the 4.11.

$$\mathbf{K_h} = \mathbf{\tilde{T_{\theta u}}^T K_\theta \tilde{T_{\theta u}}} \tag{4.14}$$

where $\mathbf{\tilde{T_{\theta u}}}$ is obtained from the equation 4.11 and K_θ can be written as function of dimensionless parameters β assembled in Q [2] as follows

$$Q_1 = \frac{2A}{3}\begin{Bmatrix} \frac{\beta_1}{l_{21}^2} & \frac{\beta_2}{l_{21}^2} & \frac{\beta_3}{l_{21}^2} \\ \frac{\beta_4}{l_{32}^2} & \frac{\beta_5}{l_{32}^2} & \frac{\beta_6}{l_{32}^2} \\ \frac{\beta_7}{l_{13}^2} & \frac{\beta_8}{l_{13}^2} & \frac{\beta_9}{l_{13}^2} \end{Bmatrix} \quad Q_2 = \frac{2A}{3}\begin{Bmatrix} \frac{\beta_9}{l_{21}^2} & \frac{\beta_7}{l_{21}^2} & \frac{\beta_8}{l_{21}^2} \\ \frac{\beta_3}{l_{32}^2} & \frac{\beta_1}{l_{32}^2} & \frac{\beta_2}{l_{32}^2} \\ \frac{\beta_6}{l_{13}^2} & \frac{\beta_4}{l_{13}^2} & \frac{\beta_5}{l_{13}^2} \end{Bmatrix} \quad Q_3 = \frac{2A}{3}\begin{Bmatrix} \frac{\beta_5}{l_{21}^2} & \frac{\beta_6}{l_{21}^2} & \frac{\beta_4}{l_{21}^2} \\ \frac{\beta_8}{l_{32}^2} & \frac{\beta_9}{l_{32}^2} & \frac{\beta_7}{l_{32}^2} \\ \frac{\beta_3}{l_{13}^2} & \frac{\beta_1}{l_{13}^2} & \frac{\beta_2}{l_{13}^2} \end{Bmatrix} \tag{4.15}$$

$$Q_4 = 1/2(Q_1+Q_2), Q_5 = 1/2(Q_3+Q_2), Q_6 = 1/2(Q_1+Q_3) \tag{4.16}$$

Using the above relations the hierarchical stiffness can be written as:

$$\mathbf{K}_\theta = A({Q_4}^T A_{m_{nat}} Q_4 + {Q_5}^T A_{m_{nat}} Q_5 + {Q_6}^T A_{m_{nat}} Q_6) \tag{4.17}$$

Combining the basic stiffness $\mathbf{K_b}$ and hierarchical stiffness $\mathbf{K}_\theta$ the complete stiffness of the element becomes

$$\mathbf{K} = \frac{3}{4}\beta_0 {\tilde{T_{\theta u}}}^T \mathbf{K}_\theta \tilde{T_{\theta u}} + K_b \tag{4.18}$$

where $\frac{3}{4}\beta_0$ is a scaling factor that depends on material invariants. For the exact derivation of the free parameter coefficients β's refer to the authors work [2]. The stiffness matrix represented in equation 4.18 takes into account the drilling degrees of freedom and will be used further in this thesis.

4.2 Inertia Relief Analysis

For an unconstrained body the stiffness matrix will be singular, therefore the traditional static analysis cannot be performed. In inertia relief case the applied load is balanced by the inertial force based on the rigid body accelerations with respect to reference point. Now that the body is in equilibrium conventional static analysis can be performed to extract the elastic responses such as displacements. Rigid body contribution is then added to it to get the final response.

Therefore the displacement of the structure can be stated as follows:

$$\mathbf{u} = \mathbf{u^e} + \mathbf{u^r} \tag{4.19}$$

where u represents the total displacement, u^r represents the rigid body part and u^e represents the elastic part. The displacement u will be vector of the size, number of degrees of freedom when implemented using finite element method. The displacement can be calculated from the equilibrium equations. The steady state equation for an unconstrained body can be given as follows:

$$[F] = [K][u] + [M][R][a] \tag{4.20}$$
$$\tag{4.21}$$

Since the body is unconstrained it undergoes rigid body accelerationRa when a force is applied. Here R is a transformation matrix which should be accounted for to accurately present the rigid body dynamics of the body. The rotation of the body around z-axis with respect origin is shown in figure 4.3, here the it can be seen that together with rotation there is also translation motion that can be expressed in terms of $\triangle z$ and $\triangle x$. Similarly rotation around x and y also causes similar translational motion.

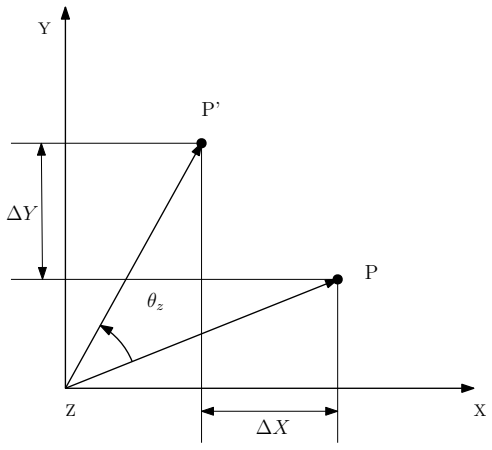

Figure 4.3: Rigid body rotation

The translation of all the points or nodes in the structure will be uniform(in the direction of force applied) but the rotation will vary with respect to reference point or point of rotation of body. With this in mind, the Rigid body matrix of a node can be stated as follows:

$$R_{node_i} = \begin{pmatrix} 1 & 0 & 0 & 0 & \triangle(z) & -\triangle(y) \\ 0 & 1 & 0 & -\triangle(z) & 0 & \triangle(x) \\ 0 & 0 & 1 & \triangle(y) & -\triangle(x) & 0 \\ 0 & 0 & 0 & 1 & 0 & 0 \\ 0 & 0 & 0 & 0 & 1 & 0 \\ 0 & 0 & 0 & 0 & 0 & 1 \end{pmatrix} \qquad R = \begin{pmatrix} R_{node_1} \\ R_{node_2} \\ \vdots \\ \vdots \\ R_{node_n} \end{pmatrix} \tag{4.22}$$

Assembling R_{node_i} for all the nodes, will give the final rigid body matrix which takes the form shown in the matrix on right side. To calculate the acceleration the steady state equation can be multiplied by R for each quantity$(K, u, MandF)$ to account for the rigid body transformation.

$$R^t F = R^t K R u + R^t M R a \tag{4.23}$$

Since the body unconstrained, $R^t K R u = 0$ as stiffness matrix is singular. The above equation can be reduced to the following form to find the acceleration of the body.

$$R^t F = R^t M R a \tag{4.24}$$

$$a = \frac{R^t F}{R^t M R} \tag{4.25}$$

With the acceleration known, the force due to acceleration MRa can be found out which is the inertial force acting on the body. At steady state the applied force and inertial force will be opposite to each other restraining the motion of the body. The applied force F and MRa can be rearranged from the equation 4.21 to find the reduced force vector F_r which is given as follows:

$$F = Ku + MRa \tag{4.26}$$

$$F - MRa = Ku \tag{4.27}$$

$$F_r = Ku \tag{4.28}$$

With the static condition achieved a conventional linear static analysis can be performed on the structure to find out the displacement due to elastic forces or internal forces . The rigid body displacements $u_r = 0$ at static condition as the body constraint. The displacement of the elastic part (u^e) will therefore be :

$$u^e = K^{-1} F_r \tag{4.29}$$

The rigid body part of the displacement u^r can be calculated by the following method. The displacements and rotations of body can represented using rigid body matrix R as follows:

$$u^r = R\alpha \tag{4.30}$$

$$u = u^e + R\alpha \tag{4.31}$$

where α is the unknown quantity. To find α, it is assumed that at steady state the average rotation and translation of the body will be zero. This can be represented by multiplying the

right hand side and left hand side of the equation 4.31 by quantity R^tM. Setting this equation to zero , the unknown α can be found:

$$R^tMu^e + R^tMR\alpha = 0 \tag{4.32}$$

$$\alpha = \frac{-R^tMu^e}{R^tMR} \tag{4.33}$$

Therefore the total displacement of the body accounting for the inertia relief forces can be represented as $u^e + R\alpha$.

4.2.1 Inertia Relief of beams

Inertia Relief of beams are modelled with beam elements. Length of the beam is $1m$ and is divided into 10 elements. A point force applied on the mid point of beam in the vertical direction. The free body diagram for the inertia relief analysis of the beam is shown below. The support point used for the static analysis step is shown by SP in the figure 4.4. A force of $1000[N]$ is applied on the middle of the beam :

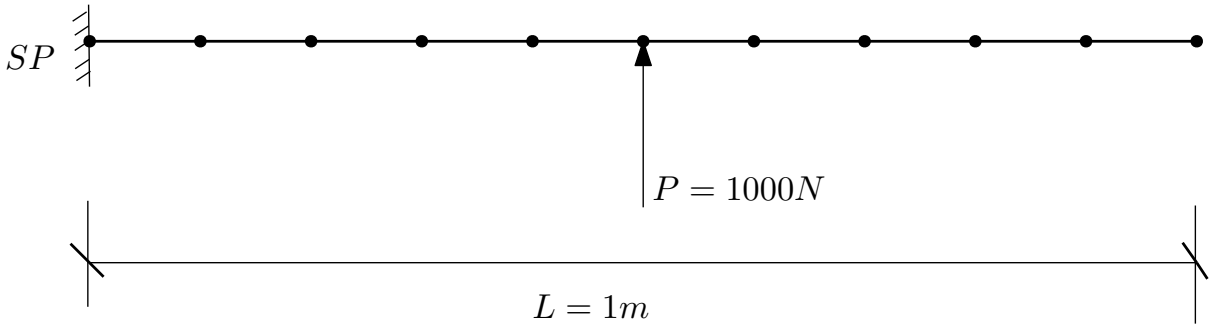

Figure 4.4: Free body diagram for inertia relief of beam

Here for the SP node all the 2 degrees of freedom will be constraint. For brevity the derivation of the stiffness matrix of beam element will not be shown. The stiffness of beam elements is well explained by authors such as Megson [43], whose representation of beam element will be adopted for this study. Beam element used here, has 2 degrees of freedom at its nodes. The vertical displacement and the in-plane rotation. The applied loads can therefore be a vertical shear load or an in-plane moment. The stiffness matrix of a beam element can be extracted from the equilibrium condition, the equilibrium condition can be stated as follows:

$$\begin{pmatrix} F_{y_i} \\ M_i \\ F_{y_j} \\ M_j \end{pmatrix} = EI \begin{pmatrix} 12/L^3 & -6/L^2 & -12/L^3 & -6/L^2 \\ -6/L^2 & 4/L & 6/L^2 & 2/L \\ -12/L^3 & 6/L^2 & 12/L^3 & 6/L^2 \\ -6/L^2 & 2/L & 6/L^2 & 4/L \end{pmatrix} \begin{pmatrix} v_i \\ \theta_i \\ v_j \\ \theta_j \end{pmatrix} \tag{4.34}$$

The above equation is of the form $[F] = [K][U]$ and the stiffness matrix of a beam element can therefore be written as:

$$K = EI \cdot \begin{pmatrix} 12/L^3 & -6/L^2 & -12/L^3 & -6/L^2 \\ -6/L^2 & 4/L & 6/L^2 & 2/L \\ -12/L^3 & 6/L^2 & 12/L^3 & 6/L^2 \\ -6/L^2 & 2/L & 6/L^2 & 4/L \end{pmatrix} \tag{4.35}$$

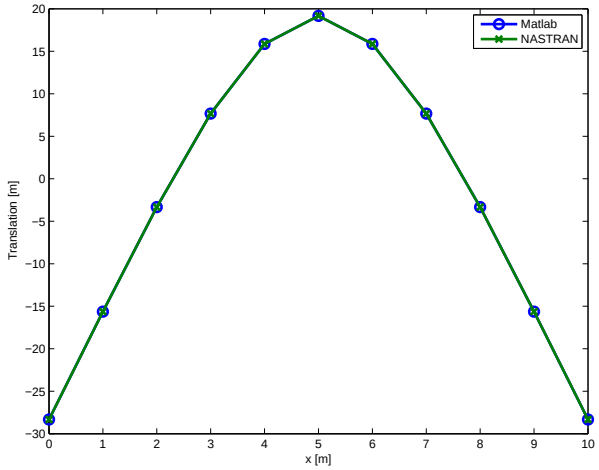

Figure 4.5: Translation of beam, [m]

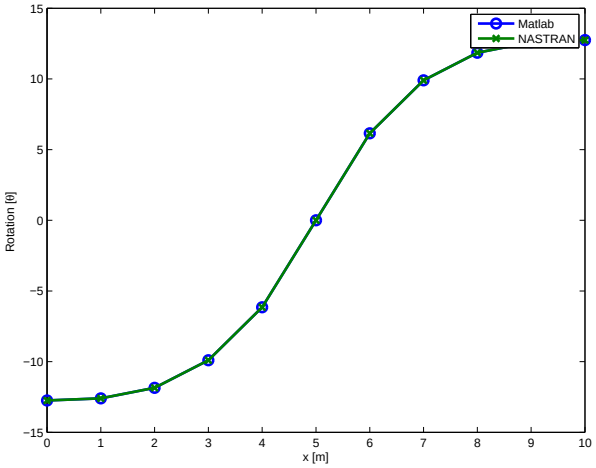

Figure 4.6: Rotation of beam, [θ]

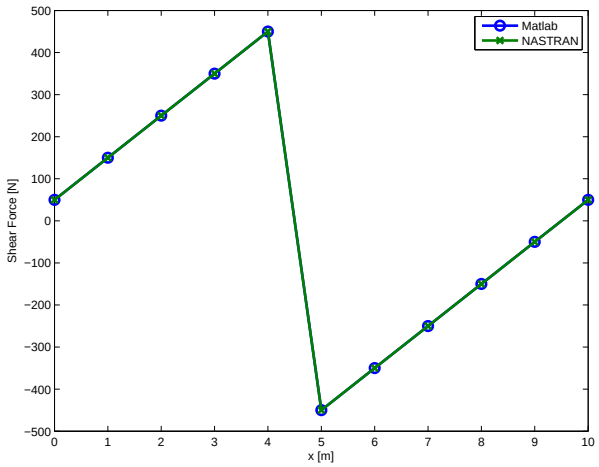

Figure 4.7: Shear Force distribution, [N]

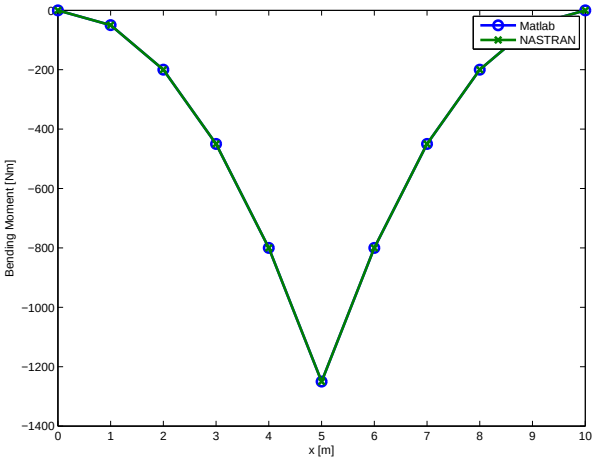

Figure 4.8: Bending Moment distribution, [Nm]

A beam of the above mentioned characteristics was modelled into MSC PATRAN/NASTRAN for the comparison. The results showed exact match, and therefore validates the approach taken to solve inertia relief analysis. Since the actual structure studied in the thesis is modelled with triangular elements, a comparison study with triangular elements is also done in the following section where the emphasis is to validate the Finite element itself.

4.2.2 Inertia Relief on panels

For inertia relief of rectangular panels a $0.6mx0.4m$ panel will be used. The plate is modelled with the higher order elements shown in the 4.1. The plate is loaded with force of $F = 800[N]$ in the x direction in the form of edge load as shown in figure 4.9. The support points shown in figure are used in static analysis step. The degrees of freedom (DOF) constraint are shown in the table 4.2.2 where the translational DOF of the support point is shown by T and the rotational DOF by R.

The results of inertia relief analysis of plates are presented here. The shell resultant force or force per width distribution are shown below where subscript x indicates normal X com-

ponent, y indicates normal Y component and xy indicates the shear component. Additional error plots are provided to indicate the real error occurring in the problem. Absolute error (the magnitude of the difference) graphs are also presented to show the intensity of the error.

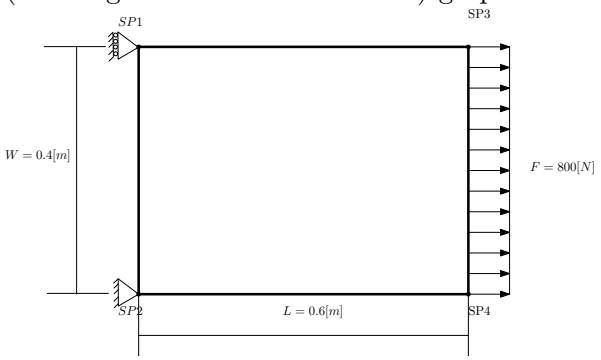

Figure 4.9: Free body diagram for inertia relief of plate

Support Points	DOFS constraint T-Translation, R-Rotation
$SP1$	T_x
$SP2$	T_x, T_y, T_z
$SP3$	T_z
$SP4$	T_z

Table 4.1: Support Conditions

In MSC PATRAN/NASTRAN the Inertia Relief Analysis can be invoked by setting **PARAM INREL − 2**. This is will perform an automatic inertia relief, here 'automatic' means that the selection of support points are done by the solver itself and no user input is required. Matching the real support point to that of MSC PATRAN/NASTRAN is not a trivial task as it is unknown to the user. Since the support point creates zero reaction force (as explained in section 4.2), a different combination of support points will provide the same result as along as the structure is not over constraint.

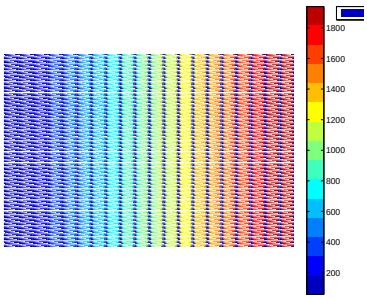

Figure 4.10: F_x from MATLAB $[\frac{N}{mm}]$

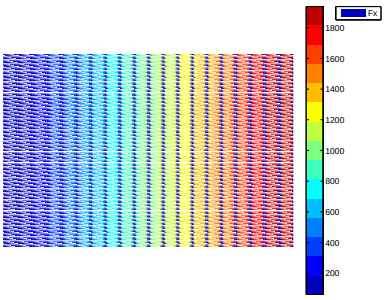

Figure 4.11: F_x from NASTRAN $[\frac{N}{mm}]$

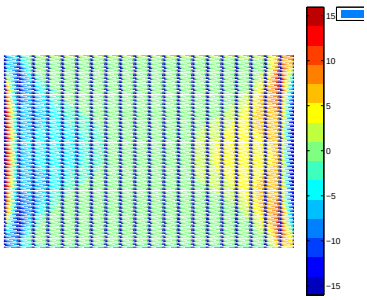

Figure 4.12: F_y from MATLAB $[\frac{N}{mm}]$

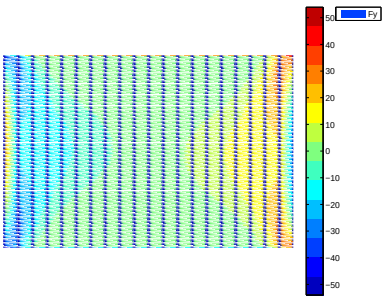

Figure 4.13: F_y from NASTRAN $[\frac{N}{mm}]$

In comparison with results from NASTRAN ,the higher order element shows sub-optimal per-

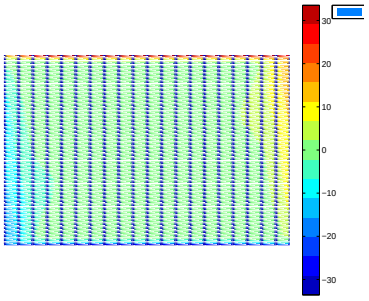

Figure 4.14: F_{xy} from MATLAB $[\frac{N}{mm}]$

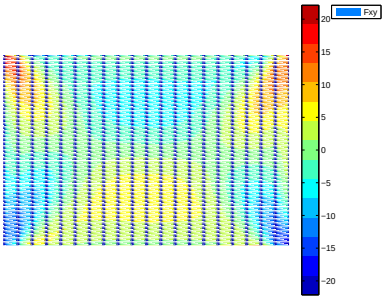

Figure 4.15: F_{xy} from NASTRAN $[\frac{N}{mm}]$

formance (in terms of values predicted) when modelled with anisotropic material which is also cited in [2]. One of the reason is because the values of optimality parameter β can become sub optimal resulting in sub optimal elements, therefore the stress is not recovered accurately. The other reason is in inertia relief, loads are distributed along the structure to counterbalance the applied force, and depending on the distribution of force (whether its too concentrated in certain nodes or more distributed over the domain) the stress correlation error can vary. When concentrated forces are used the higher order elements tends to predict higher stresses in areas where the boundary conditions are applied. Therefore a variation in the stress values compared to commercial codes are excepted for the current finite element model. The error in the finite element results are shown below, the error distribution is more concentrated on the side were force is applied (which is visible in the absolute error distribution graph).

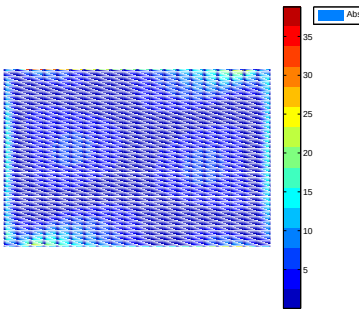

Figure 4.16: Absolute Error in F_x results, $[\frac{N}{mm}]$

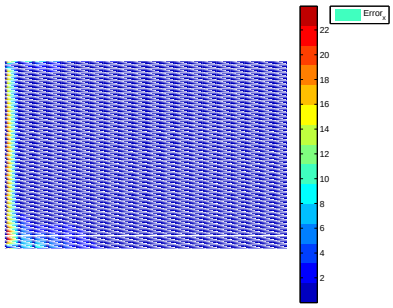

Figure 4.17: Relative Error in F_x results, [%]

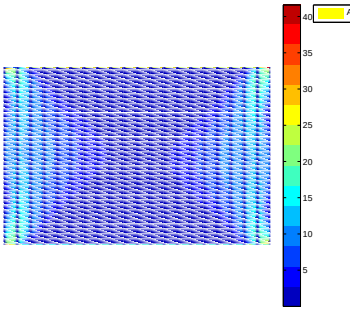

Figure 4.18: Absolute Error in F_y results, $[\frac{N}{mm}]$

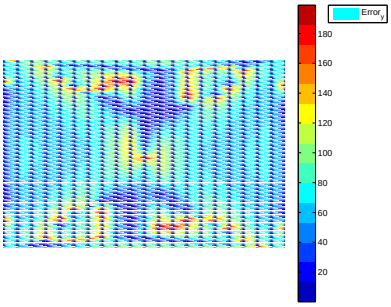

Figure 4.19: Relative Error in F_y results, [%]

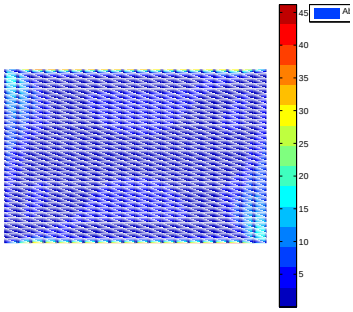

Figure 4.20: Absolute Error in F_{xy} results, $[\frac{N}{mm}]$

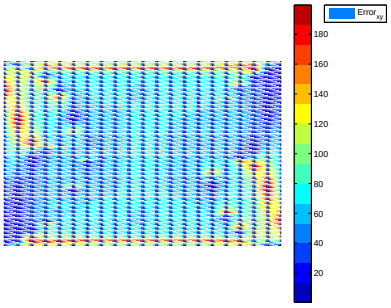

Figure 4.21: Relative Error in F_{xy} results, [%]

4.2.3 Inertia Relief on cylinders

A cylinder of height and width $0.5mx0.25m$ will be used for the inertia relief. An out of plane 'point' load is applied on the cylinder exactly in the middle at length $= 0.5m$. This load will be balanced by the inertia relief forces on the cylinder. The free body diagram of the cylinder is shown in the figure below 4.22.The support points shown in figure and the table 4.2.3 are used in static analysis step of the inertia relief. The $SP1$ is constraint in x,y,z translations, $SP2$ is constraint in x,y translation and $SP3 and SP4$ is constraint in y translation only.

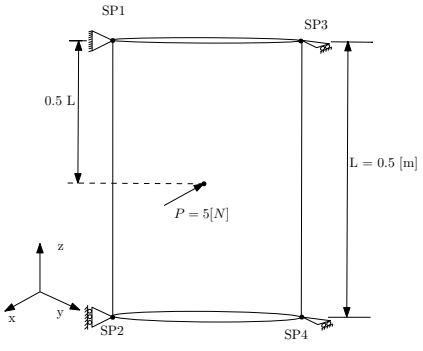

Figure 4.22: Free body diagram for inertia relief of cylinder

Support Points	DOFS constraint T-Translation, R-Rotation
$SP1$	T_x, T_y, T_z
$SP2$	T_x, T_y
$SP3$	T_y
$SP4$	T_y

Table 4.2: Support Conditions

The finite element model is constructed using higher order triangular element described in 4.1. The computed shell force resultant(force per width) F_x,F_y,F_{xy} are shown and in comparison with Nastran results.

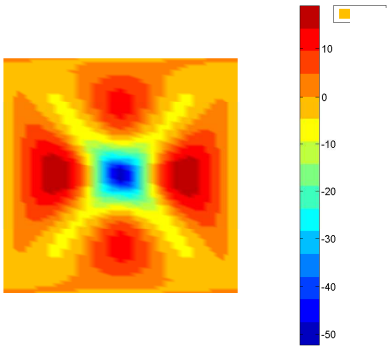

Figure 4.23: F_x Distribution on cylinder,$[\frac{N}{mm}]$

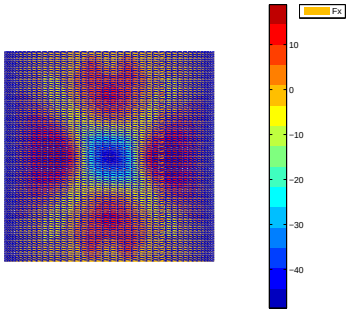

Figure 4.24: F_x from NASTRAN, $[\frac{N}{mm}]$

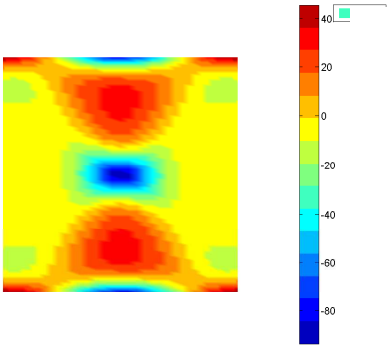

Figure 4.25: F_y distribution on cylinder, $[\frac{N}{mm}]$

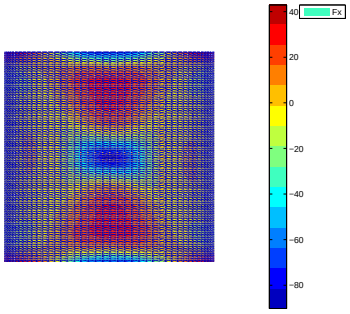

Figure 4.26: F_y from NASTRAN, $[\frac{N}{mm}]$

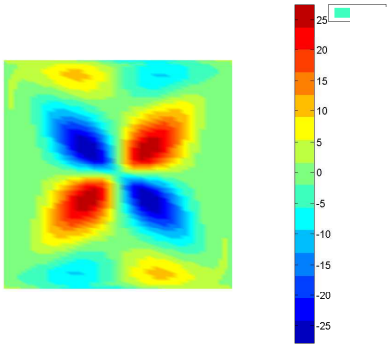

Figure 4.27: F_{xy} distribution on cylinder, $[\frac{N}{mm}]$

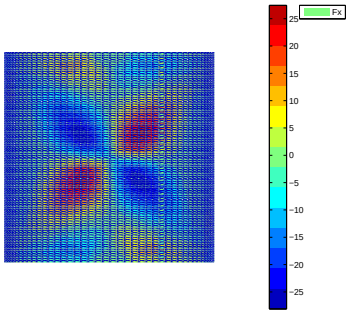

Figure 4.28: F_{xy} from NASTRAN, $[\frac{N}{mm}]$

A mesh of 90 elements across the radius and height of the cylinder is used in both Matlab and NASTRAN. The matlab results showed better agreement with the NASTRAN results as compared to the case of rectangular panel. The absolute error distribution of the problem shows maximum error near point where force is applied which is exactly in the middle of the cylinder. This behaviour is seen also with panels as discussed above due to the nature of the element formulation.

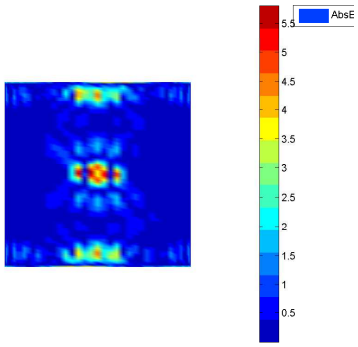

Figure 4.29: Absolute Error in F_x results,$[\frac{N}{mm}]$

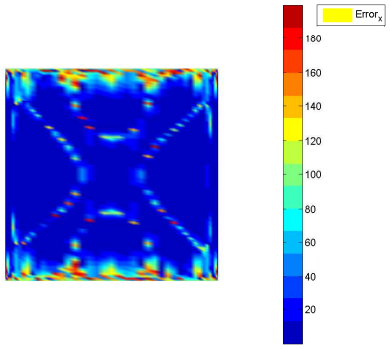

Figure 4.30: Relative Error in F_x results, [%]

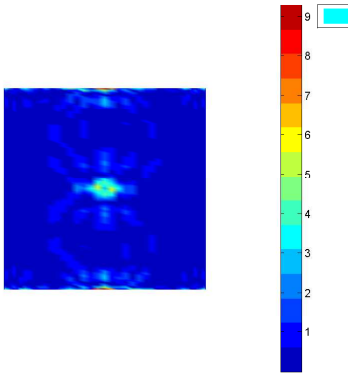

Figure 4.31: Absolute Error in F_y results, $[\frac{N}{mm}]$

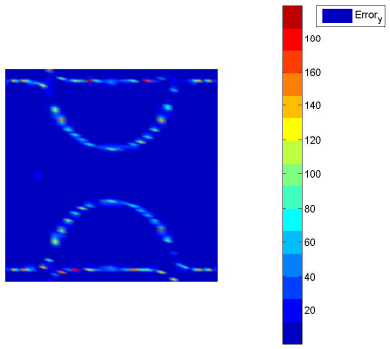

Figure 4.32: Relative Error in F_y results, [%]

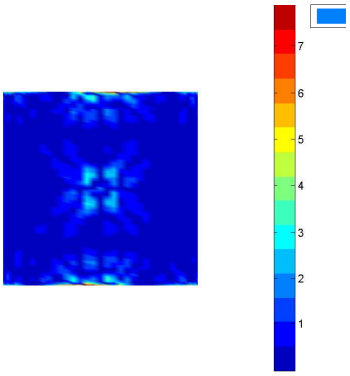

Figure 4.33: Error in F_{xy} results,$[\frac{N}{mm}]$

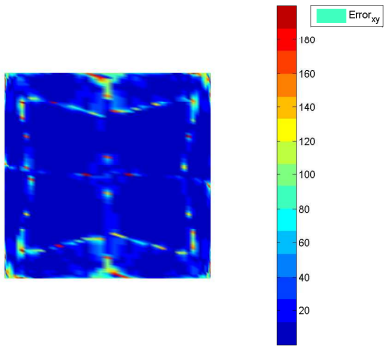

Figure 4.34: Error in F_{xy} results, [%]

4.3 Inertia Relief of DES model

Using the method discussed above for 2D finite element models, inertia relief analysis can be done for the automotive part . Model dimensions and boundary conditions were explained in the chapter 3. The load is applied through rigid body elements connected throughout the nodes on the edge 2 of the model shown in the Figure 4.35. The load is applied in X direction of the model perpendicular to the edge 2 as seen in Figure 4.35. The double curved nature of the model observed in these figures points to the fact that even though the force is applied perpendicular to structure, lateral bending can be accepted from the analysis results.

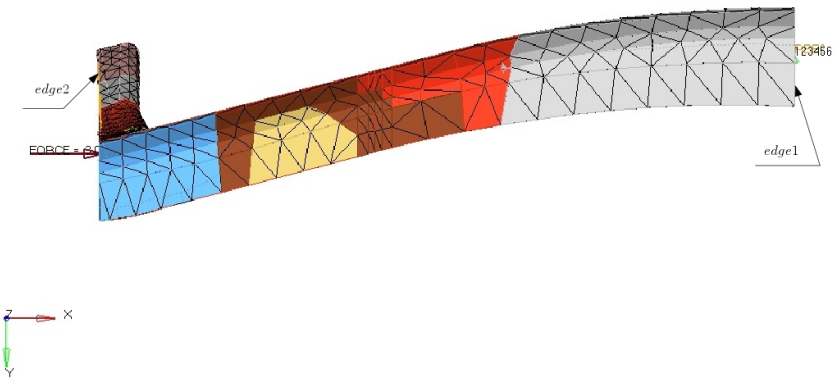

Figure 4.35: Inertia Relief Boundary condition

According to inertia relief the applied load should be balanced by the inertial load. This would mean acceleration of the body would be opposite to the direction of applied force. This equal and opposite forces should balance the structure and at the same time create a bending stress. This effect can be seen in the shell force resultant (or force per length) result shown in Figure 4.36 and Figure 4.37. Here the top side of the structure is in compression and the bottom side is in tension. The results from both hypermesh and matlab shows similar stress distribution. It can also be noted that the regions with higher stress corresponds to the regions with high thickness seen in Figure 3.3 in the previous chapter. This is essentially due to the use of optimized

laminates obtained from Hypermesh. The optimization has added thickness to the region with higher stress and reduced the thickness in lower stress regions. It can also be noted that the higher stresses are very local, concentrated near the curved section of the structure.

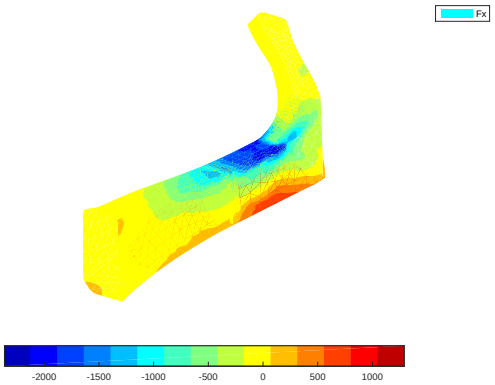

Figure 4.36: F_x from Matlab, $[\frac{N}{mm}]$

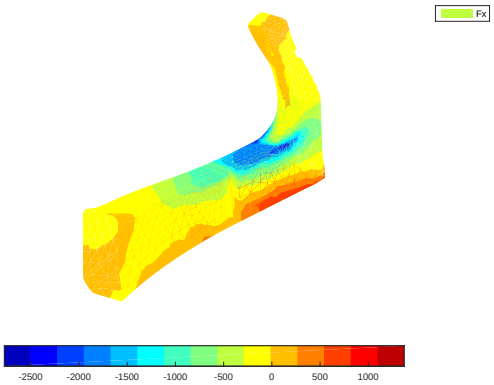

Figure 4.37: F_x from Hypermesh, $[\frac{N}{mm}]$

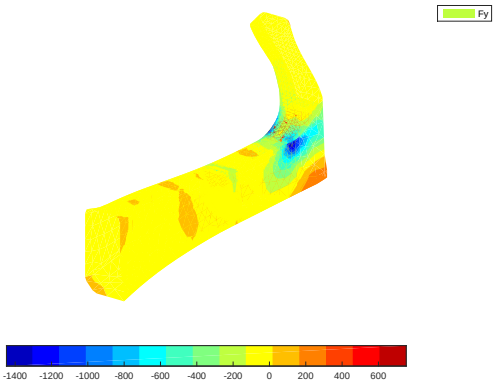

Figure 4.38: F_y from Matlab, $[\frac{N}{mm}]$

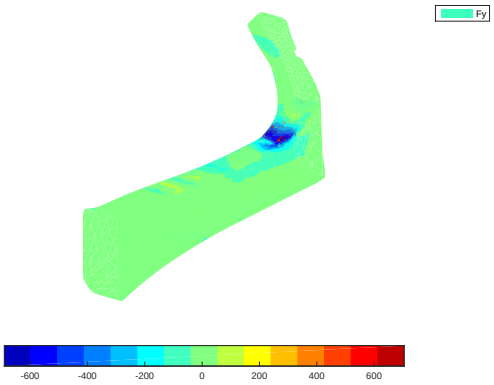

Figure 4.39: F_y from Hypermesh, $[\frac{N}{mm}]$

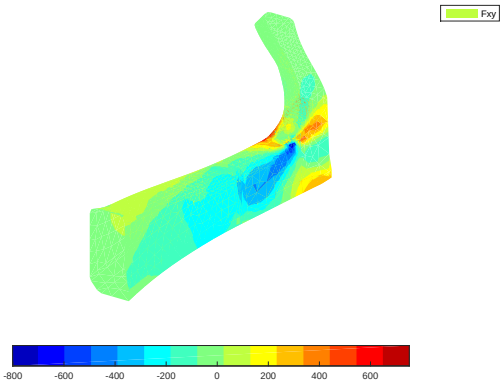

Figure 4.40: F_{xy} Matlab, $[\frac{N}{mm}]$

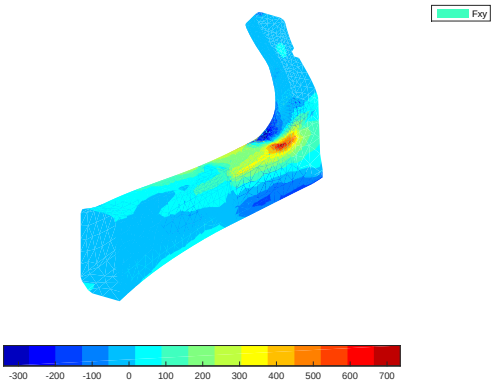

Figure 4.41: F_{xy} Hypermesh, $[\frac{N}{mm}]$

The error in the results from matlab as compared to Hypermesh are shown in Figure 4.42 to Figure 4.47. The error plots follows the pattern seen in the case of cylinder and panel. The absolute error graphs helps to show that the error is local. As have been seen before the error seems to concentrate near the boundary conditions. In the case of inertia relief the applied loads are on the edge and higher errors are seen near the edge2. Here a coarse mesh is used for the analysis to reduce the number of design points in optimization. This ofcourse has an effect in the quality of the results. But the general distribution of the results shows a global agreement which can be seen from F_x results Figure 4.36.

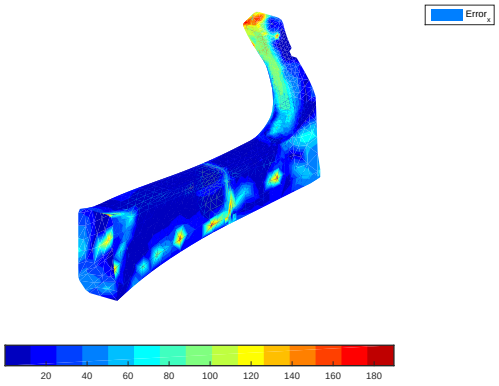

Figure 4.42: Relative Error in F_x results, [%]

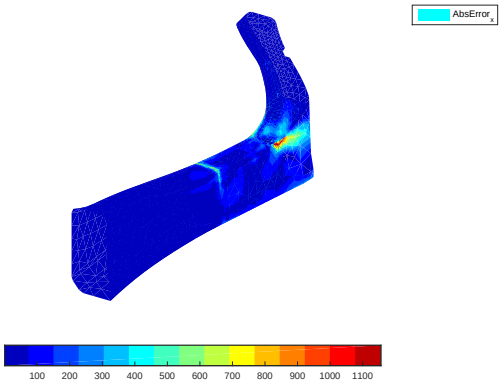

Figure 4.43: Absolute Error in F_x results, $[\frac{N}{mm}]$

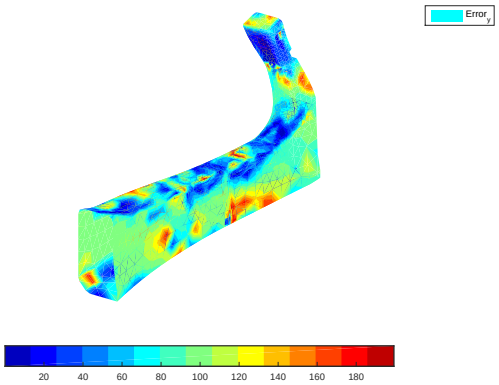

Figure 4.44: Relative Error in F_y results, [%]

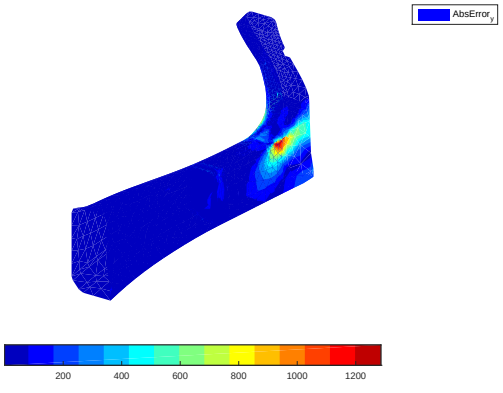

Figure 4.45: Absolute Error in F_y results, $[\frac{N}{mm}]$

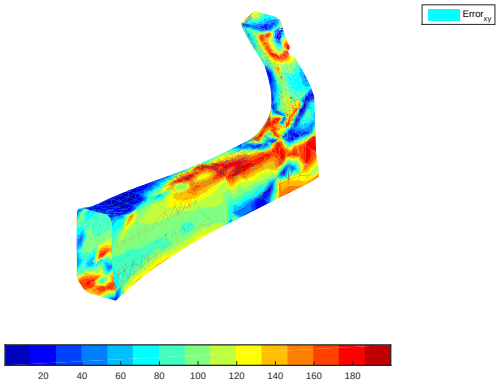

Figure 4.46: Relative Error in F_{xy} results, [%]

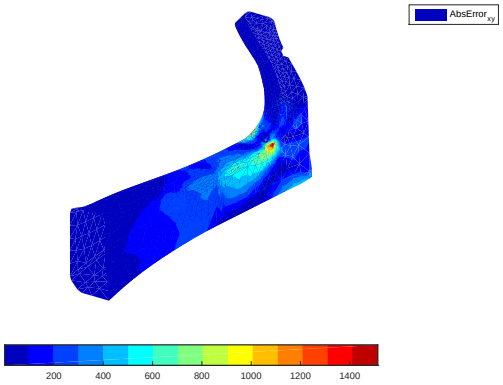

Figure 4.47: Absolute Error in F_{xy} results, $[\frac{N}{mm}]$

Chapter 5

Optimization Setup

The optimization setup for DES model will be explained in this chapter. The interior-point method as explained Section 2.4.1 is the basis for the optimization. The min-max optimization problem for DES model is shown below:

$$\begin{aligned} min \quad & max(f_1, f_2, ..., f_n) \\ s.t \quad & f_{n+1}, ...f_m \leqslant 0 \\ & \varsigma^2 - \varsigma_U^2 \leqslant 0 \end{aligned} \tag{5.1}$$

here f represents the normalized inverse structural responses. The calculation of structural responses were discussed in the chapter 2. The normalization procedure for these responses are shown in the coming section.

As mentioned before there are 2 loadcases studied in this thesis, inertia relief and bending loadcase. An FEA is performed for each case and the needed responses are calculated. For the inertia relief case, strength (σ) and compliance (C) responses are of interest. The design is critical in strength when inertia relief loads are applied therefore strength will be taken as the objective for the optimization. The Compliance for this loadcase will be given as an constraint. And for the Bending case, compliance and buckling responses are calculated. This loadcase is the least critical of the two and therefore the responses are set as constraints. The objectives and constraints for the optimization as per the requirements are summarized below:

Loadcase	Objectives	Constraints
Inertia Relief	Strength	Compliance
Bending	-	Compliance, Buckling

Table 5.2: Optimization objectives and constraints

The critical responses from the conventional laminate based DES model will be selected for normalization. Objective of the optimization (which is strength responses) is evaluated at every node. Therefore the critical response will be node with critical stress($\sigma_{critical}$) or high failure

index (r). But since during the optimization the critical node may change, a conservative approach will be to select a range of nodes with higher failure index values. The number of critical nodes does influence the computational time therefore only nodes with relatively higher stress levels are taken. For the current DES model a set of 54 nodes needs to be selected which shows higher stress values. Critical regions can be identified from the shell force resultant result shown in section Section 4.3.

In the Table 5.4 maximum stress out of these critical nodes are given. For buckling the critical buckling load out of the two modes will be selected for normalization. Compliance value is global, therefore for each load case there will be only one value. Responses from the conventional design is summarized in table Table 5.4,

Loadcase	Max(Strength)	Compliance	Max(Buckling mode)
Inertia Relief	0.5060	$2.87e^5$	-
Bending	-	$2.85e^4$	0.0408

Table 5.4: Critical Responses for the conventional laminate design for DES model

Normalized Responses

The responses used in the thesis are normalized with respect to a initial design value denoted by subscript 0. The responses stated in the above section will therefore be transformed into the following normalized form:

$$C_{norm} = \frac{C_{design}}{C_0} \tag{5.2}$$

$$r_{norm} = \frac{r_{design}}{r_0} \tag{5.3}$$

$$P_{cr} = \frac{P_{cr}}{P_{cr0}} \tag{5.4}$$

Parameters for the setup of optimization is once again summarized below:

1. Objectives : strength (Inertia relief loadcase)
2. Constraints : stiffness & buckling
3. Global Steering : $3m^{-1}$
4. No. iterations limit : 40
5. Convergence criteria level two approximation(interior point method) : $1e^{-}3$
6. Convergence criteria level one approximation(FEM) : $5e^{-}3$

The global steering constraint limits for AFP is $3m^{-1}$ [1] and for TFP there are no limits. Global steering is the sum of steering radius of all the elements averaged over the area of the domain. Therefore its applied per layer rather than per element.

Once the responses are calculated the sensitivities can be obtained for each node in the domain. The sensitivities are calculated using the adjoint method. The formulation of the sensitivities are

outside the scope of this thesis , readers are referred to the work of Daniël Peeters [1]. Once the sensitivities and responses are calculated the multi-level approximation method can be initiated. As mentioned in Section 2.4.1 a two level approximation is made for implementing the interior point method. The approximations for DES model follows the same method, with the level one approximation formulated using convex linearization approach. Level one approximation can be expressed in terms laminate stiffness matrices **A** and **D** as follows:

$$f^{(1)} = \sum_{n} \phi_m : \mathbf{A}^{-1} + \phi_b : \mathbf{D}^{-1} + \psi_m : \mathbf{A} + \psi_b : \mathbf{D} + c \tag{5.5}$$

As explained before ':' operator represents a Frobenius inner product ($A : B = trace(A^T \cdot B)$), coefficients of the reciprocal and linear approximation terms ϕ and ψ are computed from the sensitivity analysis [22]. The above approximation is always convex and free term c is the constant part which is zero if there is no inhomogeneous part for the function. However for the problem in hand there are constant parts which are not optimized so the homogeneity condition is violated. Therefore the constant parts needs to be excluded from the optimization. Since f represents responses, taking the constant part out would create a different structure and therefore different response will be obtained. A method to bypass this problem is explained in the coming section.

Constants in Level one approximation

The constant parts in the finite element model are the inner baffle parts. The function value of nodes (denoted by n_c) connecting these parts are taken out of the level one approximation and reassigned to the constant c^*. Although these nodes are nodes are not optimized they cannot be entirely taken out of the optimization as it will effect function value at the approximation point. It is to be noted that at approximation point the responses and structural approximations have to be the same according the conditions specified in the section 2.4 . To make the condition valid the new constant c^* can be formulated as follows:

$$c^* = \sum_{n_c} \phi_m : \mathbf{A}^{-1} + \phi_m : \mathbf{D}^{-1} + \psi_b : \mathbf{A} + \psi_b : \mathbf{D} \tag{5.6}$$

The above change in value of c will be added to the level one approximation which retains the function value validity at approximation point. This can be checked by comparing the FEM response and level one function. The level one approximation can be rewritten as the summation of the nodes $n - n_c$:

$$f^{(1)} = \sum_{n-n_c} \phi_m : \mathbf{A}^{-1} + \phi_m : \mathbf{D}^{-1} + \psi_b : \mathbf{A} + \psi_b : \mathbf{D} + c^* \tag{5.7}$$

The level two approximation is derived from the level one approximation in terms of fiber angles. The level one was expressed in terms of stiffness matrices, for the level two approximation the level on is written in terms of fiber angles as design variables.

$$f^{(2)} = f_0^{(1)} + \mathbf{g} \cdot \Delta\theta + \frac{1}{2}\Delta\theta^T \cdot \mathbf{H} \cdot \Delta\theta \tag{5.8}$$

Here (g) and (H) is the gradient and Hessian of the level one approximation at the approximation point.

Damping functions are added to make conservative approximations. The damping functions stated in section 2.4.1 has been adapted for the DES model. The damping function is created by taking into account only for the optimized nodes.

Level two update rule for DES model

The update is done for level one and level two approximations using above specified method. However it was noticed that the level two approximation for the *DES* model was non-conservative and required large number of iterations. Here the damping function was recalculated in each iteration using the equation 2.56 based on the newly found optimum. This damping factor was found to be maintaining the conservativeness and there were no large oscillations in the approximation values.

$$\zeta^{new(2)} = \frac{1}{2} \cdot \mathbf{g}^T \cdot \mathbf{H_d}^{-1} \cdot \mathbf{g} \tag{5.9}$$

The lagrangian of the problem takes the same form as discussed in the Section 2.4.1. Lagrangian is constructed in terms z normalized vector (z) and manufacturing constraints

$$\begin{aligned} \mathcal{L}(\lambda_0, \lambda_c, \theta, z, s_0, s_c) = z + \lambda_0 \cdot (f - z \cdot e^T + s_0) \\ +\theta^T \cdot (\lambda_c \cdot \mathbf{L}) \cdot \theta - \varsigma_U{}^2 \cdot (\lambda_c \cdot |\Omega|) \\ +\lambda_c \cdot s_c |\Omega|) \\ -\mu \cdot (\ln(s_0) + |\Omega| \cdot \ln(s_c)) \end{aligned} \tag{5.10}$$

where λ_0 and λ_c are the lagrange multipliers of the functions(i.e responses) and constraints. And homotopy factor is depicted by μ. To find the optimal point the gradient of the Lagrangian has to be set to zero. The gradient is calculated with respect to $\lambda_0, \lambda_c, \theta, z, s_0, s_c$. After finding gradients and setting it to zero, optimization follows the method discussed in 2.4, where linearized set of equations are solved to find updated variables.

For this optimization problem the convergence criteria is defined as follows:

level two function convergence:

$$Corrector_{new} - Corrector_{old} \leq 1e^{-3} \tag{5.11}$$

level one function convergence:

$$f^1_{new} - f^1_{old} \leq 5e^{-3} \tag{5.12}$$

Convergence is obtained when the improvement from the old value is minimal. The convergence criteria selected here is of the order 1^{-3}, which is sufficiently low enough to make sure that there is no further significant improvement. This doesn't mean a global optimum point is found as outcome, the optimal point will still be a local optimum.

Chapter 6

Results & Discussion

To investigate the feasibility of the variable stiffness laminates design for DES model, it is necessary to prove that the variable stiffness design will be an improvement compared to the conventional design. Therefore an optimization problem is setup with the input parameter coming from the conventional design provided in the Section 3.1. As explained before normalized values are used for optimization, in this test case the basis for normalization will be the responses from conventional laminate design (which is the initial response or response at approximation point). This way a comparison can be drawn by looking at the improvement in normalized objective function.

Results obtained after the optimization is given in the table below. The optimization was continued until the 40th iteration instead of using a stopping criteria, this does mean that there can be local minimum's appearing in the objective function. The objective function improved from 0.78 to 1.65 which is a significant improvement. The constraints are not violated throughout the optimization which can be noticed from the Table 6.1 as the values are not falling below the starting point. In fact some improvement can be observed in constraints as well (although minimal).

Discussion of the optimization results: The optimization definitely showed the improvement in mechanical properties by using variable stiffness laminates. The objective of the optimization was to improve the strength of the structure as compared to a conventional laminate design which has been achieved. The stiffness and buckling were the constraints whose values improved by a small margin compared to initial value . Therefore it can be said that the preliminary goals of the optimization and the thesis has been sufficiently met, with a $2x$ improvement in the objective value.

A closer look at optimization results show that the objective values are getting trapped in local minimums. However a stable value has been reached from 20th iteration onwards and the change in objective values is insignificant. In this test case the optimization is allowed to run until number of iteration limit that is 40. The fiber angle distributions have been changed compared to initial uni-directional design, this can be seen in figures given the coming section.

Iteration	Optimal normalized Strength	Optimal normalized Stiffness	Optimal normalized Buckling mode 1	Optimal normalized Buckling mode 2
Start	0.78	1.00	1.00	1.117
1	1.0050	1.1349	1.0084	1.1329
2	1.0431	1.111	1.0058	1.1245
3	1.2706	1.0891	1.0285	1.1519
5	1.4424	1.0350	1.0148	1.1346
10	1.6388	1.0077	1.0091	1.1348
15	1.6603	1.0036	1.0094	1.1378
20	1.6453	1.0036	1.0077	1.1357
30	1.6440	1.0098	1.0079	1.1360
40	1.6453	1.0098	1.0079	1.1360

Table 6.1: Optimization Results in terms of normalized responses

6.1 Fiber path representation

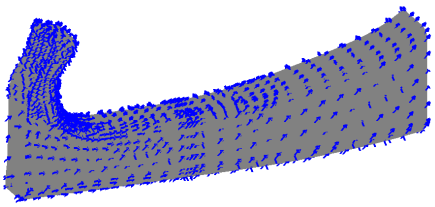

Figure 6.1: optimized fiber angles for layer 1

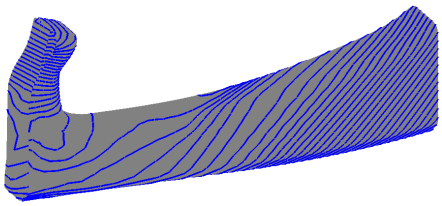

Figure 6.2: optimized fiber paths for layer 1

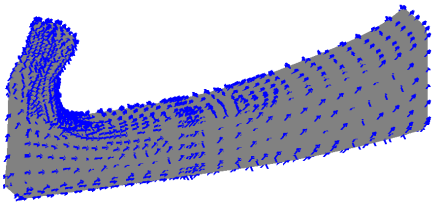

Figure 6.3: optimized fiber angles for layer 2

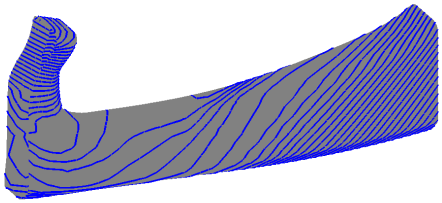

Figure 6.4: optimized fiber paths for layer 2

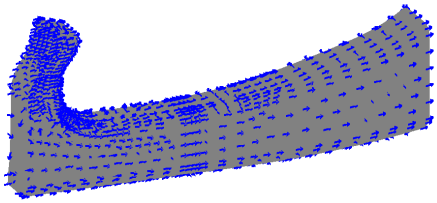

Figure 6.5: optimized fiber angles for layer 3

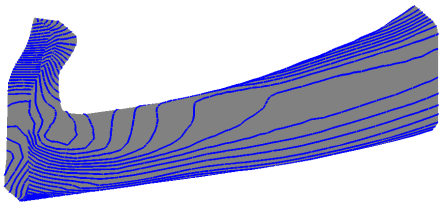

Figure 6.6: optimized fiber paths for layer 3

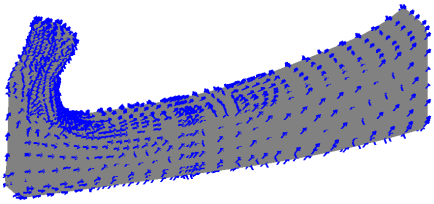

Figure 6.7: optimized fiber angles for layer 4

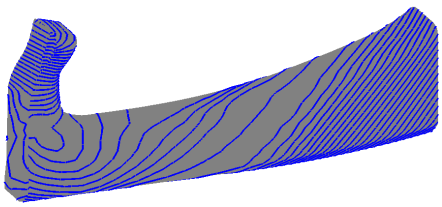

Figure 6.8: optimized fiber paths for layer 4

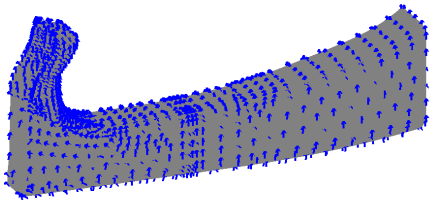

Figure 6.9: optimized fiber angles for layer 5

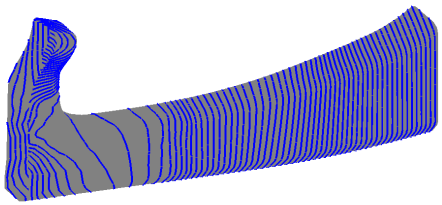

Figure 6.10: optimized fiber paths for layer 5

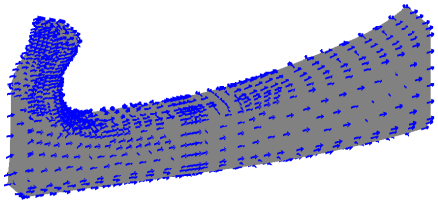

Figure 6.11: optimized fiber angles for layer 6

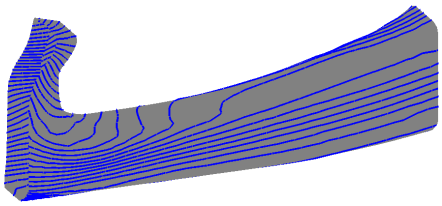

Figure 6.12: optimized fiber paths for layer 6

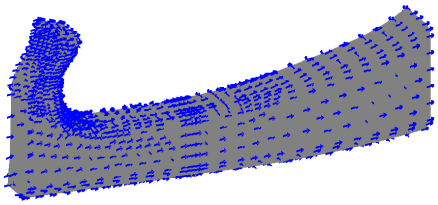

Figure 6.13: optimized fiber angles for layer 7

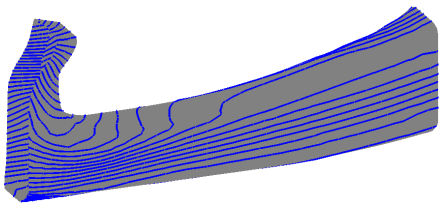

Figure 6.14: optimized fiber paths for layer 7

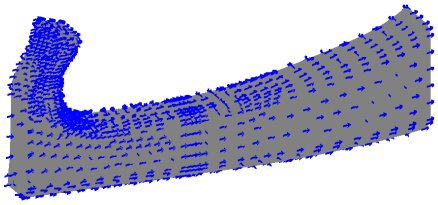

Figure 6.15: optimized fiber angles for layer 8

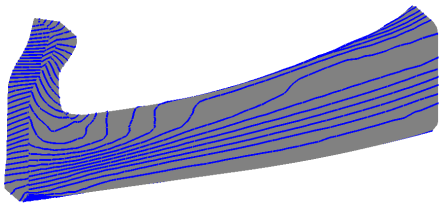

Figure 6.16: optimized fiber paths for layer 8

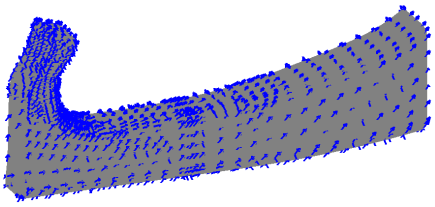

Figure 6.17: optimized fiber angles for layer 9

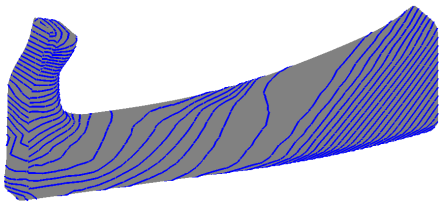

Figure 6.18: optimized fiber paths for layer 9

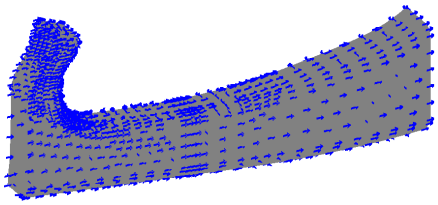

Figure 6.19: optimized fiber angles for layer 10

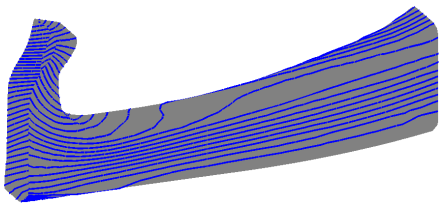

Figure 6.20: optimized fiber paths for layer 10

Discussion of the fiber path result: The fiber paths shown above are the results of streamline curve fitting of fiber angles based on the work of A.W Blom [18]. The streamlines represents the direction of flow of fiber angles. It can be seen that there are certain regions in the model where the fiber paths are not generated or fiber paths seems to diverge. These paths represent change in direction of fiber angles along the direction of the fiber path. Looking at the fiber paths of layer 1 which was initially 45° layer, it can be seen that the top side of model tends to be aligned with 45° but as it moves to lower surface the fibers straightens towards 0°. This can be explained looking at the loadcases, for instance in the inertia relief case the model is essentially in compression due to the compressive force. The curved nature of the structure should bend the structure making top surface to be in compression and bottom surface to be in tension. From this point of view it is beneficial to add more 0° layers to bottom to increase strength in tension, which is what the optimization results are showing.

If the layer 4 which was initially 0° layer is observed, it can be seen that there are similar change in top and bottom surface. On the top surface the angle changes from 0° to 45°. Moving towards the bottom surface the change direction is minimal, and it remains at 0° . It can be seen that optimization is indeed trying to increase the strength in these critical areas according to its loading state.

Had the objective of the optimization been stiffness , it would have been more beneficial to add 45° layers away from the neutral axis or the symmetry line which increases the bending stiffness which however is not the case since stiffness is not the objective but constraint. This is a sign that optimization is indeed trying to improve strength of the structure and the results are in the right direction.

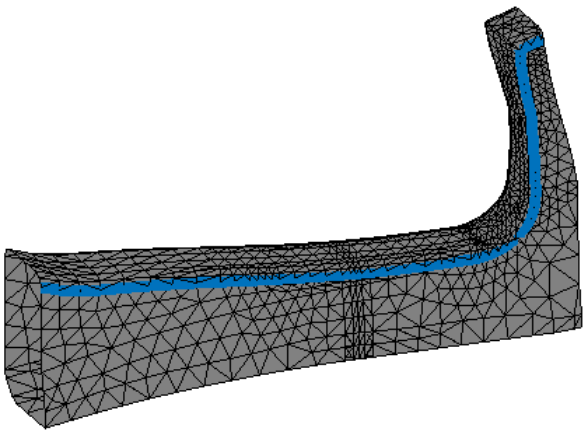

Figure 6.21: Inflow and Outflow boundary for fiber paths

The other interesting feature here is the presentation of streamlines itself. Streamlines needs an inflow boundary and an outflow boundary to accurately find path connecting angles. A closed surface cannot be used for generating streamlines as it doesn't have distinct inflow and outflow boundary. For generation of the streamlines the model is cut open so that it becomes a open surface rather than closed surface. This artificially creates a inflow and outflow region, shown in Figure 6.21 with blue line. In an ideal case the fiber path trajectory shouldn't effect the performance of the structure , but as discussed in Section 2.5 the real structures are prone

to defects such as gaps and overlaps due to the way composite tapes are cut at boundaries during manufacturing. These regions will cause stress concentrations effecting the mechanical performance of the structure. Looking at the fiber paths it can be seen that divergence and convergence of the fiber paths will potentially create gaps and overlaps in the design. Therefore the inflow and outflow boundaries needs to taken in such a way that minimal defects will be created.

One way to bypass the problem will be by increasing the number of inflow and outflow regions. This will split the surface into multiple sub regions giving more freedom for generating smooth fiber paths. Splitting the surface into multiple regions to generate fiber paths independently and then stitching them together during manufacturing would be ideal for these structures. This would also give greater freedom and flexibility in manufacturing. Therefore an additional post processing step is required to further improve the fiber path representation. The effects of multiple inflow and outflow boundaries are not investigated in this thesis, but recommended for the future research.

Chapter 7

Conclusion

The variable stiffness optimization of the automotive structure was done during this thesis. One of the important task was to add Inertia Relief analysis capabilities to finite element part which is required to implement the inertia relief loadcase. This goal was achieved and responses from inertia relief were used for optimization of the structure. The developed method was tested on simple structures such as beam, panel and a cylinder. The inertia relief result of beam model showed exact correlation, however for $2D$ element models of plate and cylinder the quality of the correlation is poor owing to the usage of triangular elements. This effects was also seen in DES model since it is also modelled by $2D$ triangular elements. However it should be noted that the correlation issues are local, a general agreement for FEM results are achieved if a global distribution of the stresses are considered.

The optimization procedure was largely based on the multi-level gradient based optimization method developed by researchers from TU Delft such as IJsselmuiden [20] and Peeters [1]. The optimization function was setup to meet DES model requirements by taking into account influence of optimized and non-optimized parts. Once the setup was complete a fiber angle optimization was successfully done and the fiber paths were generated.

Optimization showed the potential of variable stiffness laminates which was one of the research questions for this thesis. The results showed that significant improvement can be achieved from the conventional laminate design. For the DES model with initial layup shown in Section 3.1 almost twice the improvement was observed for the objective value which was the failure strength of the model. The constrained responses which were stiffness and buckling load of the model remained below the constraint values. The fiber paths boundaries were created by splitting open the surface which created inflow and outflow boundaries. The fiber path is observed to be following the expected optimization results. The top part of the model which is in compression is dominated by 45° and the bottom part which is in tension is dominated by 0°. Although it can be seen that physical representation of the fiber path plots can be improved if the number inflow and out-flow boundaries were to be increased.

It can be concluded that the research questions addressed in this thesis has been answered quantitatively, the thesis showed that improvements can be achieved in mechanical properties such as strength and stiffness of the structure by using a variable stiffness design. Inertia relief analysis capabilities has also been added to the FE part. Considering the quality of the results obtained in this thesis certain recommendation has to be made for further research and effective usage of variable stiffness design method discussed here.

7.1 Recommendations

In the chapter 4 where the finite element model was formulated it can be seen that the triangular element results are met with correlation errors when compared with results from commercial software(Hypermesh and MSC Nastran). This is caused due to the linearized formulation of the triangular elements presented in that chapter. Considering the magnitude of errors in the results, a better formulation of triangular element is required for gaining confidence in FEM results. An alternative solution would be to use quad elements.

Construction of the approximations are done by manually separating optimized and non-optimized parts during calculation. This can be labour intensive process for structures with large number of parts. Therefore a method that can automatically separate these parts during optimization would be effective in saving pre-processing time.

The responses calculated assumes a perfect laminate without any gaps and overlaps or resin rich areas. In a real structure, these effects tends to influence the responses of the structure as indicated in the study of Pasini et.al [17]. Therefore a better formulation of local mechanical defects by using a micro-mechanical model or stochastic models can bring FEM results closer to real structures. Also the non-linearity effects are not considered as only linear static analysis is done for calculating responses. The non-linear effects should also be considered if better understanding of the behaviour of the structure is desired.

The other assumption made in the analysis is the plain-stress effect. Considering the highest thickness of the laminate found in the model is 12 mm it should be noted that laminates are no longer thin. Therefore influence of out-plane stresses will also dictate the responses in real-world structures. Influence of delamination and inter-laminar stresses should be taken into account to avoid build up of residual stresses in laminates (that can be induced during manufacturing). This can be implemented by changing the stiffness formulation and imposing additional strength constraints ($\sigma_z < \sigma_{zallowable}$).

For the optimization part, which is only focused on fiber angle optimization can be extended to thickness optimization which can bring further improvement. Although, this task would involve considering the effects of change in inertia relief loads during optimization. It can be seen that the inertial relief loads are function of mass and shape (rigid body modes), therefore sensitivities of these factors needs to be calculated for a topology optimization or a variable thickness optimization. Pagaldipti et.al [16] studied about the influence of inertia relief on optimal designs and has found that the optimal designs with and without the sensitivities of shape results in different optimal designs. Therefore the current optimization setup should be extended to include these effects for topology. This can potentially bring weight savings to the current design by optimizing the thickness.

References

[1] D.M.J Peeters. *Design Optimization of practical variable stiffness and thickness laminates.* PhD thesis, 2017.

[2] C. A Felippa. A study of optimal membrane triangles with drilling freedoms. *Computer Methods in Applied Mechanics and Engineering*, 192(16âĂŞ18):2125 – 2168, 2003.

[3] S. Setoodeh, M.M. Abdalla, and Z. Gürdal. Design of variable–stiffness laminates using lamination parameters. *Composites Part B: Engineering*, 37(4):301–309, 2006.

[4] A. Khani, S.T. IJsselmuiden, M.M. Abdalla, and Z. Gürdal. Design of variable stiffness panels for maximum strength using lamination parameters. *Composites Part B: Engineering*, 42(3):546–552, 2011.

[5] S. Setoodeh, M.M. Abdalla, S.T. IJsselmuiden, and Z. Gürdal. Design of variable-stiffness composite panels for maximum buckling load. *Composite structures*, 87(1):109–117, 2009.

[6] M.M. Abdalla, S. Setoodeh, and Z. Gürdal. Design of variable stiffness composite panels for maximum fundamental frequency using lamination parameters. *Composite structures*, 81(2):283–291, 2007.

[7] D.H.A Lukaszewicz, C. Ward, and K.D. Potter. The engineering aspects of automated prepreg layup: History, present and future. *Composites Part B: Engineering*, 43(3):997–1009, 2012.

[8] P.J. Crothers, K. Drechsler, D. Feltin, I. Herszberg, and T. Kruckenberg. Tailored fibre placement to minimise stress concentrations. *Composites Part A: Applied Science and Manufacturing*, 28(7):619–625, 1997.

[9] D.M.J. Peeters and M.M. Abdalla. Effect of steering limit constraints on the performance of variable stiffness laminates. In *ICCM 20: 20th International Conference on Composite Materials, Copenhagen, Denmark, 19-24 July 2015*. ICCM, 2015.

[10] D.M.J Peeters, S. Hesse, and M.M Abdalla. Stacking sequence optimisation of variable stiffness laminates with manufacturing constraints. *Composite Structures*, 125:596 – 604, 2015.

[11] C. Kassapoglou. *Design and analysis of composite structures: with applications to aerospace structures*. John Wiley & Sons, 2013.

[12] H. T. Hahn and S. W. Tsai. *Introduction to composite materials*. CRC Press, 1980.

[13] M.W Bloomfield, C.G Diaconu, and P.M Weaver. On feasible regions of lamination parameters for lay-up optimization of laminated composites. *Proceedings of the Royal Society of London A: Mathematical, Physical and Engineering Sciences*, 465(2104):1123–1143, 2009.

[14] S. Setoodeh, Z. Gürdal, and L. T. Watson. Design of variable-stiffness composite layers using cellular automata. *Computer Methods in Applied Mechanics and Engineering*, 195(9âĂŞ12):836 – 851, 2006.

[15] J.M.J.F. van Campen, C. Kassapoglou, and Z. Gürdal. Generating realistic laminate fiber angle distributions for optimal variable stiffness laminates. *Composites Part B: Engineering*, 43(2):354 – 360, 2012.

[16] N. Pagaldipti and Y.K Shyy. Influence of inertia relief on optimal designs. *Multidisciplinary Analysis Optimization Conferences*, 2004.

[17] M.A. Nik, K. Fayazbakhsh, D. Pasini, and L. Lessard. Optimization of variable stiffness composites with embedded defects induced by automated fiber placement. *Composite Structures*, 107:160–166, 2014.

[18] A.W. Blom. *Structural performance of fiber-placed, variable-stiffness composite conical and cylindrical shells*. PhD thesis, 2010.

[19] A. de Wit and F. van Keulen. Numerical comparison of multi-level optimization techniques. page 1895, 2007.

[20] S. T. IJsselmuiden. Optimal design of variable stiffness composite structures using lamination parameters. *PhD diss., Delft University of Technology*, 2011.

[21] C. Fleury. Conlin: An efficient dual optimizer based on convex approximation concepts. *Structural optimization*, 1(2):81–89, 1989.

[22] R. T Haftka and Z. Gürdal. *Elements of structural optimization*, volume 11. Springer Science & Business Media, 2012.

[23] K. Svanberg. A class of globally convergent optimization methods based on conservative convex separable approximations. *SIAM journal on optimization*, 12(2):555–573, 2002.

[24] R.J. Grone and M.N. Grimshaw. Composite tape laying machine with pivoting presser member. December 09 1986. US Patent 4,627,886.

[25] W. Goldsworthy, E. Hardesty, and H. Karlson. Geodesic path length compensator for composite-tape placement head. May 14 1974. US Patent 3,810,805.

[26] T. Martinez. Fiber tow connectors for tape laying(faserstreifenverbinder fuer bandwickler). Patent DE 10 2008 010 424 A1, 2008.

[27] R. Calawa and J. Nancarrow. Medium wave infrared heater for high-speed fiber placement. SAE Technical Paper, 2007, 2007.

[28] A. Hamlyn and Y. Hardy. Fibre application machine with a tool changing system, 2008. WO Patent App. PCT/FR2008/050,808.

[29] M.A. Lamontia and M.B. Gruber. Limitations on mechanical properties in thermoplastic laminates fabricated by two processes: automated thermoplastic tape placement and filament winding. In *Proceedings of the 26th International SAMPE EUROPE Conference*, pages 5–7, 2005.

[30] J. Sloan. Atl and afp: Defining the megatrends in composite aerostructures. *Composite World: High Performance Composites*, 16(4):68–72, 2008.

[31] D.H.A. Lukaszewicz. *Optimisation of high-speed automated layup of thermoset carbon-fibre preimpregnates*. PhD thesis, University of Bristol, 2011.

[32] A. Jacob. Hexcel ready to fly on the a350 xwb. Reinforced Plastics Volume 57, Issue 3, May-June 2013, p25-26, 2013.

[33] D. Emerson, D. Grauer, B. Hangs, M. Reif, F. Henning, A. Martsman, A.B. Oxeon, and S.T. Jespersen. Using unidirectional glass tapes to improve impact performance of thermoplastic composites in automotive applications. 2012 SPE ACCE Conference, 2012.

[34] P. Mattheij, K. Gliesche, and D. Feltin. 3d reinforced stitched carbon/epoxy laminates made by tailored fibre placement. *Composites Part A: Applied Science and Manufacturing*, 31(6):571–581, 2000.

[35] E.G. Koricho, A. Khomenko, T. Fristedt, and M. Haq. Innovative tailored fiber placement technique for enhanced damage resistance in notched composite laminate. *Composite Structures*, 120:378–385, 2015.

[36] H. Temmen, R. Degenhardt, and T. Raible. Tailored fibre placement optimization tool. 25th International Congress of Aeronautical Sciences, 2006.

[37] A. Spickenheuer, A. Leipprand, L. Bittrich, K. Uhlig, E. Richter, and G. Heinrich. Process-dependent material properties for structural simulation of composites made by tailored fibre placement. ECCM16 - 16TH European conference on composite materials, Seville, Spain, 22-26 June, 2014.

[38] G. Gardiner. Tailored fibre placement : Besting metal in volume production. High Performance Composites,Composite World,Septmeber, 2013.

[39] E. Richter, K. Uhlig, A. Spickenheuer, L. Bittrich, E. Mäder, and G. Heinrich. Thermoplastic composite parts based on online spun commingled hybrid yarns with continuous curvilinear fibre patterns. In *16th European conference on composite materials*, 2014.

[40] T. Saito, J. Hiramoto, and T. Urabe. A study of optimization for automotive parts and structures by using inertia relief. *Structural and Multidisciplinary Optimisation*, 11, 2015.

[41] A. Majid and B. Babak. Automotive body fatigue analysis âĂŞ inertia relief or transient dynamics? In *SAE Technical Paper*. SAE International, 09 1999.

[42] M. F Nelson and J. A Wolf. The use of inertia relief to estimate impact loads. In *SAE Technical Paper*, pages 149–155. SAE International, 02 1977.

[43] T.H.G. Megson. *Aircraft Structures for Engineering Students*. Elsevier aerospace engineering series. Elsevier Science, 2007.